

Ca' Foscari University

Graduating student

**Teresa Scovacricchi** 877501

Internal supervisor

**Francesca Caterina Izzo**

External supervisors

**Koen Janssens**

**Alba Álvarez Martín**



# MALDI–MSI: A new method for studying the degradation of historical organic pigments

Master's degree programme of Conservation Science and Technologies for cultural heritage

Academic year 2020/2022

## MALDI–MSI: A new method for studying the degradation of historical organic pigments

The aim of the thesis is to study the light–induced degradation process of eosin lakes or geranium lakes by MALDI – MSI (Matrix Assisted Laser Desorption Ionization–Mass Spectrometry Imaging). Geranium lakes are eosin–based organic red pigments used by Van Gogh and his contemporaries. To investigate its behavior, a forced aging treatment was performed by exposing directly geranium lake oil paint to sunlight over a 100–day time span. The model samples were created in the laboratory to reproduce the paints used by the artists. Attenuated Total Reflection Infrared (ATR–FTIR), X–ray Powder Diffraction (XRPD) and Positive Electrospray Ionization Time–of–flight Mass Spectroscopy (TOF–MS–ES +) were the techniques employed for the preliminary characterization in the laboratory of simple systems such as pure pigments without binders. In addition, the advancement of degradation was monitored in real time using non–invasive analyzes such as fiber optic reflectance spectroscopy (FORS) and microscopic analyzes. The results obtained using MALDI–MSI analysis provide innovative spatial information never exploited in the field of cultural heritage. However, when studying the cross sections of a paint, a major challenge in this project was the optimization of the protocol for sample preparation prior to data collection. Within each section, thanks to MALDI–MSI, it is possible to obtain details on the lateral distribution of the main key molecule analyzed: eosin, the secondary products formed during its degradation process and any third molecules linked to the interaction between the different components of the pictorial system: oil, pigment (lead white) and chromophore (eosin). The study of the spatial distribution of the different compounds identified in the samples analyzed during the aging process and a posteriori has provided us with new information on the behavior and degradation of this pigment over time.

## Acknowledgements

*It was a troubled and non-linear university journey.*

*My thanks go first and foremost to my family, the backbone of my person. Remembering my sharp and brilliant grandmother whom I hope to make proud.*

*The friends I found along the way made even the most challenging moments precious.*

*Marco who made every milestone special.*

*I am grateful for the opportunities I received thanks to Professor Janssens. The fundamental leadership of Alba allowed me to arrive safely at the end of this journey and far beyond the limits of my imagination. Ermanno's kindness helps me to not feel alone along the way. I would also thank Jusai Quanico and all the members of the AXIS and ARCHES groups.*

# INDEX

1. Introduction
2. Analytical techniques employed
  - 2.1. XRD analysis
  - 2.2. Microscope particle size evaluation
  - 2.3. ATR–FTIR analysis
  - 2.4. ESI–MS
  - 2.5. FORS
  - 2.6. MALDI–MSI
    - 2.6.1. MALDI sample preparation
      - 2.6.1.1. Embedding
      - 2.6.1.2. Preparation thin sections
      - 2.6.1.3. Conductive Carbon tape optimization
      - 2.6.1.4. Matrix deposition
      - 2.6.1.5. Matrix selection
      - 2.6.1.6. Calibrant
      - 2.6.1.7. MALDI–MSI analysis
3. Synthesis materials
  - 3.1. Red lakes
    - 3.1.1. Eosin
    - 3.1.2. Madder
    - 3.1.3. Brazilwood
    - 3.1.4. Cochineal
  - 3.2. Lead white
4. Microscope particle size evaluation
  - 4.1.1. Eosin
  - 4.1.2. Lead white
5. ATR–FTIR analysis of eosin
6. Molecular characterization by ESI–MS– solvent optimization
7. XRD analysis for lead white
8. Oil absorption value
9. Preparation oil paints
  - 9.1. Pigments and additives
  - 9.2. Eosin: %
  - 9.3. cochineal: %
10. Monitoring total color change through data analysis
11. MALDI–MSI analyses
  - 11.1. Results
  - 11.2. Discussion
12. Future perspectives
13. References
14. Appendix

# 1. Introduction

In 1874, BASF (Badische Anilin- & Soda-fabrik, Germany) introduced to the market a new dye suitable for silk called eosin [1]. During the following years, its use expanded into other sectors as a dye for food[2], make-up and more recently for histology research and photovoltaic cells[3]. The colorant is a tetra-brominated xanthene molecule while the pigment is obtained by dye precipitation with a coordination metal salt like aluminum or lead (Fig. 1) and it is codified as Acid Red 87 with C.I. 45380.

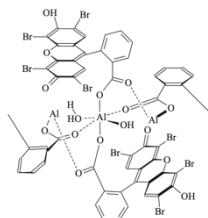


Figure 1. Eosin pigment molecular structure with aluminum[4]

After industrial revolution, it was commercialized from 1880 onwards as Geranium Lake, characterized by a bright red hue. Van Gogh, in a correspondence with his brother Theo, used to order various red lakes, fundamental for his stylistic goals[5, 6]. From the letters, we can deduce how the poor performances of these lakes were already known to the painter himself (Fig. 2)[7].



Figure 2. 593 Br. 1990: 595 | CL: 475, From: Vincent van Gogh, To: Theo van Gogh, Date: Arles, on or about Thursday, 5 April 1888 [7]

The process of lakes pigment degradation has been documented in multiple works of the artist's later production and subsequently studied in the laboratory[5, 8, 9]. One of the most important examples of the use of eosin within van Gogh's later production is *The bedroom* series(1888–1889)[10] and another significant example is *Field with Irises* near Arles (1888) [9]. For all the examples cited, there is direct testimony from the author, who describes the dyes as purplish and lilac, whereas today the dye appears light blue or deep blue.

The scientific literature reports that discoloration process is favored by light and the presence of oxygen, which causes the progressive loss of bromine from the xanthene ring[11]. By means of UV-Vis, IR, Raman spectroscopy and electrochemical experiments, it was possible to trace key information on the discoloration process of a pictorial layer containing eosin[12–14]. Mass spectrometry, on the other hand, made it possible to obtain the degradation pattern by determining the molecular composition of the products of the debromination process in real samples[15].

Since the aim is to increase knowledge of the use of eosin in the artistic context and since eosin, as a pigment, was used in oil production, it was decided to create a model with known composition and concentration to simulate a pictorial layer as far as possible. In this

way, it will be possible not only to study the molecule of interest but to verify its behavior in presence of the main materials present within a painting.

The aim of this thesis is to enrich the knowledge of the process by using the high resolution MALDI-MSI to study oil cross sections.

Mass spectrometry imaging analysis will provide spatial information of the molecules of interest. The main challenges encountered during the research were the optimization of the sample preparation and the analysis parameters. Firstly, to track how the pigment persists in the paint layer over time and secondly the distribution of its degradation products. The behavior of different species is compared to study similarities and differences in order to trace their pattern in space and afterwards in time.

The research initially focuses on the creation of samples from raw materials and their characterization. Subsequently, the samples were subjected to the drying and light ageing process under controlled conditions. The optimization of the sample for MALDI analysis and the matrices used were obtained by successive attempts, which allowed us to gain experience for the future. Finally, mass spectra were acquired, and data processed.

## 2. Analytical techniques employed

### 2.1. Microscopic evaluation

The purpose of the optical microscope is to magnify the details of the specimen under examination. Microscopic systems provide an image characterized by magnification, resolution, and contrast. The investigation parameters involved a 10- to 50-fold magnification in the dark field of the ECLIPSE LV100D microscope configured with the LV-UEPI illuminator in dark-field (Nikon).

### 2.2. ATR-FTIR analysis

The Infrared spectroscopy provides qualitative information on the molecular nature of various materials exploiting the specificity of the transition energies of the vibrational motions associated with different functional groups. The purpose of using this technique was to characterize the products obtained during the synthesis of the pigment from the dye. Using this technique, it was possible to distinguish between eosin Y and complexed eosin. ATR-FTIR analysis were carried out at the Rijksdienst voor het Cultureel Erfgoed (Amsterdam) with a Frontier FTIR + Spotlight 400 FTIR, Imaging in transmission on diamond cell with 15 scans.

### 2.3. TOF-MS and TOF-MS/MS

The time-of-flight mass spectrometry involves the ionized sample into positive ions by forcing a solution of the sample through a small, heated capillary in an electric field to produce a fine mist of charged droplets, and in which sample ions with different masses are accelerated to the same kinetic energy. The time taken by each ion to reach a detector at a known distance is measured, thus obtaining the ion's mass-to-charge ratio [16].

### 2.4. XRPD analysis

X-Ray Powder Diffraction is a method for measuring the X-Rays scattered by a polycrystalline sample as a function of crystal structures and atomic spacing. Analysis of this distribution gives a lot of information about the microstructure and properties of the crystalline latter of the samples. The used instrument is a built-in XRPD setup employing a monochromatic copper source  $\mu\text{S}$  (Incoatec, Geesthacht, Germany;  $\text{Cu-K}\alpha$ : 8.04 keV). The X-Ray generation was operated at 50 kV and a current of 1000  $\mu\text{A}$  with beam spot probing the sample with sizes of  $1 \times 0,3 \text{ mm}^2$ . A planar imaging detector (Pilatus 200K, Dectris, Villigen, CH) was employed to collect diffraction patterns, the acquisition time was set to 10s, and the final patterns is a result of 10 diffractograms collected in 10 different point and averaged.

This technique is based on the interaction of the incident X-rays with the sample, giving rise to constructive interference when conditions satisfy Bragg's Law ( $n\lambda = 2d \sin \theta$ ).

The two-dimensional (2D) X-ray patterns collected at each acquisition point were azimuthally integrated to one-dimensional (1D) diffractograms employing XRDUA a software developed by the university of Antwerp. The crystalline phases in the 1D pattern were identified by comparing the data with a powder diffraction database, taking into account the observed diffraction peak positions ( $2\theta$  angles) and their relative intensities. After integration, fitting was performed on the 1D diffractograms using a Rietveld model containing the information to allow semi-quantitative analyses.

## 2.5. FORS

FORS (Fiber Optics Reflectance Spectroscopy) has been used for art examination and art conservation for inorganic and organic pigments and dyes. The strength of this method is the relatively simplicity of the equipment: a source of light, a spectrometer and 2 fibers optics, one to deliver the light on the object and the other to collect the light reflected. The FORS spectrum shows the ratio between the intensity of the reflected light and the intensity of the incident light for each wavelength. The built-in FORS is composed by Avalight-HAL, Avantes fiber optics cables with small tip probe and 45° probe holder, AvaSpec-2048 spectrometer and Avasoft2 software. Subsequently, the spectra obtained were converted into .csv files and analysed. The chemometric investigation was conducted within Rstudio using the R-guide, applying cluster analysis and principal component analysis (PCA).

## 2.6. MALDI-MSI



It is a cutting-edge technology tool for two-dimensional MS that can visualize the spatial distribution of molecules without extraction, purification, and separation of the sample and its components [18, 19]. After collecting a mass spectrum at one spot, the sample is moved to reach another region, until the entire sample is scanned in a raster format. By choosing a selection of masses in the resulting spectra that correspond to the studied organic pigment, the data is used to map its distribution across a multi-layered sample. This results in images showing the distribution of this compound pixel by pixel [20, 21].

### 2.6.1. MALDI-MSI sample preparation






#### 2.6.1.1. Embedding

Samples were collected at 0 days, 7 days, 40 days, and 107 days. The next step was to test the use of resins to encase the sample in order to protect it and to make it easier to obtain thin sections the next step was to experiment with the use of a resin to encase the specimen in order to protect it and to make it easier to obtain thin sections [8, 22]. Various techniques and materials were considered and tried out (Table 1) [23–25]. Considering the results of IR analysis, the uncomplexed eosin contained in the samples is diffused into the liquid phase, for this reason, the possibility of embedding in ice was also discarded. The most encouraging initial results were obtained with Technovit 2000 LC, an acrylate resin. After waiting about two days, however, the diffusion of the dye was noticed by the naked eye. We therefore proceeded with several tests using the blue light polymerization device using the lowest temperature curing procedure (70° C) but all proved unsatisfactory.

Table 1. Embedding tests results

Resin		Result
Tecnovit 5000		Failure
Technovit 4004		Failure



Acrifix Liquid				Failure
VersoCit-2 Liquid				Failure
Technovit 2000 LC	day 1	day 2	day 3	Failure
				

### 2.6.1.2. Preparation of thin slides

Since embedding attempts were unsatisfactory, it was decided to proceed with the sample without pretreatment illustrated in Figure 3. The system adopted consists of enclosing the paint layer between two support sheets, one where it dried and the second cleaned and cut by the operator. The system is held under pressure and in position by the microtome's clamps while the blades move perpendicular as Figures 4 and 5 exemplify[26].

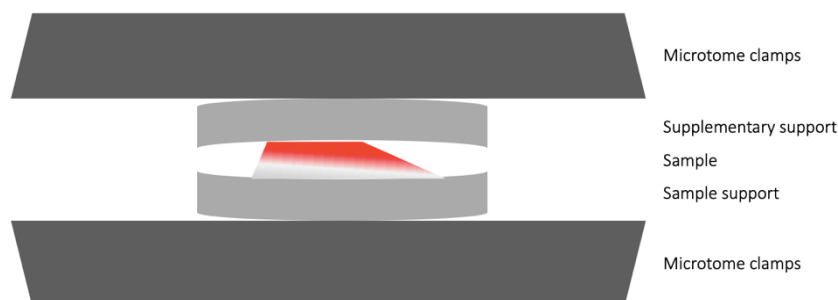


Figure 3. Microtome set-up scheme

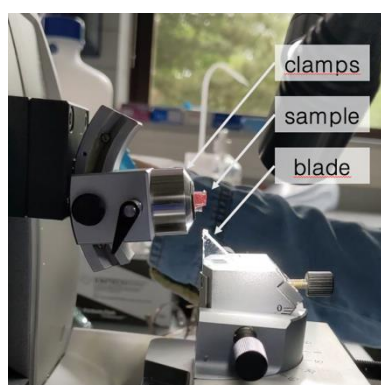


Figure 4. Photography of microtoming step

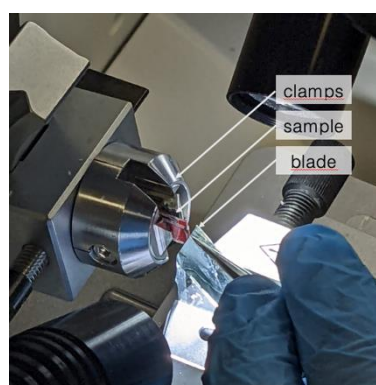


Figure 5. Photography of microtoming step

Using the microtome configured with a sharp glass blade (HistoCore NANOCUT R, Leica) 10- $\mu\text{m}$  sections of the paints were obtained in order to guarantee the perfect readability. Glass knives are made by scoring and breaking a square glass in order to obtain two triangular pieces with a 45° angles sharper edges each[24]. Each sample was mounted on double-sided conductive tape mounted previously on indium/tin oxide-coated slides (ITO, LaserBioLabs, Sophia-Antipolis, France). Given the thickness of the sample, the assembly of the plate as flat as possible was fundamental to obtain a good analysis. Different thin sections (2 or more) of the same sample were deposited on the tape to ensure the probability of obtaining surfaces suitable for analysis (Fig. 6).

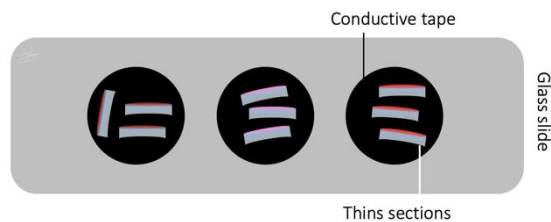





Figure 6. MALDI-MSI glass slide scheme

### 2.6.1.3. Conductive Carbon tape optimization

Different double tapes were tested in order to obtain the best analysis set-up (Table 2). The best performances were obtained by the aluminum core carbon tape due to its smoother surface but also carbon tabs were used for the analyses.

Table 2. Different used tapes

High purity conductive double sided adhesive carbon tabs	Super smooth conductive double sided carbon tabs	Double adhesive conductive carbon tape with aluminum core
		
(Micro to Nano, Innovative microscopy supplies, Haarlem, Netherlands)	(Micro to Nano, Innovative microscopy supplies, Haarlem, Netherlands)	(ITO, LaserBioLabs, Sophia-Antipolis, France)

#### 2.6.1.4. Matrix selection

The matrices considered for the analyses are shown in the Table 3[20, 27] according to literature and the laboratory availability. Since the matrix is known to affect desorption/ionization upon laser ablation[19, 28, 29] different trials were performed. The most effective working conditions were guarantee with DHB.

Table 3. Available matrixes for analysis

Matrix after literature	Abbreviation	(+)	(-)	Main applications
2,5-dihydroxybenzoic acid	DHB	X	X	o Detection of lower-weight molecules like peptides, nucleotides, oligonucleotides, and oligosaccharides, that do not ionize well with CHCA or SA
9-aminoacridine	9-AA		X	o Detection of low-weight molecules such as lipids and metabolites
norharmane	NOR	X	X	o Detection of a broad range of molecules
$\alpha$ -cyano-4-hydroxycinnamic acid	CHCA	X		o Detection of middle-weight molecules such as peptides that are smaller than 5000 Daltons
3,5-dimethoxy-4-hydroxycinnamic acid	Sinapinic acid	X		o Detection of high-weight molecules like proteins that are larger than 5000 Daltons
1,5-diaminonaphthalene	DAN, Naphthalene diamine	X	X	o Used for high spatial resolution lipid imaging

#### 2.6.1.5. Matrix deposition

2,5-dihydroxybenzoic acid (Sigma Aldrich) was sublimated onto the sections at 140 °C for 13 min using a sublimator (Thermo) set up in-house, which leads to an average of 0.424 mg matrix deposited per cm<sup>2</sup> based on three independent measurements[30] (Fig. 7).

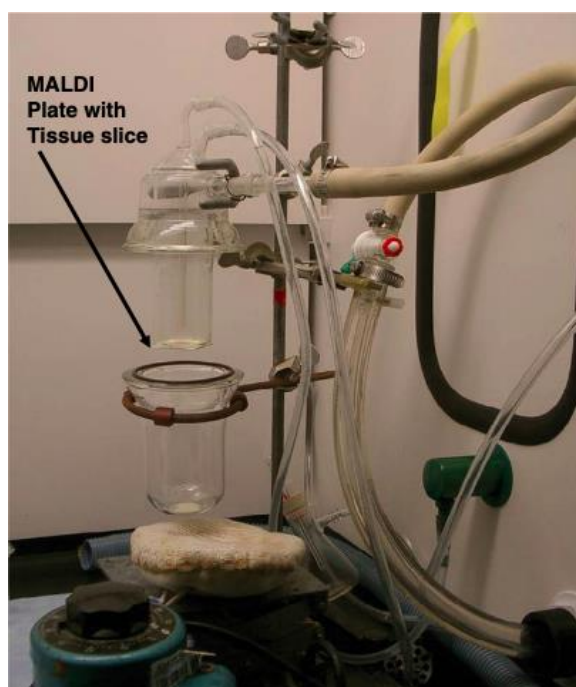


Figure 7. Matrix deposition scheme[30]

#### 2.6.1.6. Calibrant and set-up

MS imaging of tissue slices was performed using a RapiFlex MALDI TOF instrument (Bruker Daltonics, Bremen, Germany). Images were acquired at 10- $\mu$ m resolution scanning at  $m/z$  300–2.000 with the Smartbeam 3D laser firing at a frequency of 10 kHz. Each spectrum was recorded after accumulating 500 laser shots per spot. The ion source voltage was set to 20 kV, while the PIE and lens were at 2.570 and 11.600 kV, respectively. The reflectors were set at 20.800, 1.085 and 8.700 kV. Matrix suppression by deflection up to  $m/z$  240 was activated. The reflector detector gain, and sampling rate were kept constant on all imaging acquisitions. External calibration in the positive mode was performed using Peptide Mix 6 calibration standard (LaserBio Labs)[18].

#### 2.6.1.7. MALDI-MSI analysis

The acquired MS images were uploaded in SCiLS Lab version 2016b (Bruker Daltonics). The baseline was removed using the top hat method. The ion distributions of the pigments were mapped by plotting the signal intensities in all spectra normalized against the total ion count. Subsequently, orthogonal matching pursuit (OMP) was used to detect peaks; these peaks were aligned to the mean spectrum by centroid matching and automatic spatial segmentation was performed by using the bisecting k-means algorithm followed by application of weak hotspot removal. These ion distributions were plotted at  $\pm 0.300$  Da  $m/z$  intervals, with the masses reported as the maximum value in each interval. A first overview of the spatial regions of the eosin pigment (using the isotopic peak at  $m/z$  648) was achieved by applying hierarchical clustering on the MSI data of images of paint samples containing 100%, 95%, 50% and 5% eosin/Pb white. The depth of clustering was selected interactively. Receiver Operating Characteristic (ROC) analysis was performed to detect  $m/z$  values which discriminate between 100% eosin and 5% eosin and vice versa, with AUCs  $\geq 0.75$  considered significant.

### 3. Synthesis of materials

#### 3.1. Synthesis of red lakes

##### 3.1.1. Eosin

The synthesis of eosin was conducted following the procedure indicated by Ana Claro [8] as follow. In a basic demineralized water solution (pH=12), eosin Y (99% dye content, Sigma–Aldrich) is dissolved in a concentration of about 3 mM under stirring (Fig. 8). When the complete dissolution occurs, a precise quantity of aluminum chloride hexahydrate,  $\text{AlCl}_3 \cdot 6\text{H}_2\text{O}$  (Sigma Aldrich) is added (see Table 4)(Fig. 9). After a sedimentation period of approximately one hour (Fig. 10), the solution is filtered through a paper filter, and let it dry completely (Fig. 11). The pigment is removed from the paper filter, grounded in a mortar, and stored in darkness until the use (Fig. 13).



Figure 8. Eosin Y dissolved in basic water

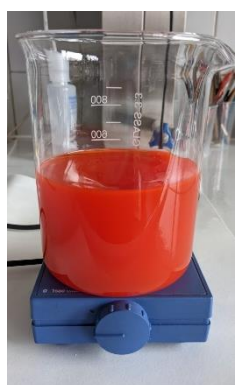


Figure 9. Aluminum chloride added to the solution



Figure 10. Sedimentation process



Figure 11. Dried powder on the filter



Figure 12. Washing waters



Figure 13. Oil paint obtained by the pigment

The key step is the addition of the aluminum salt (Fig 9) in the progressive addition. It should imply a color change from a pinkish red to a deep red. This color change was difficult to identify, from the first grain of aluminum salt added the solution. It appeared cloudy with a color between orange and red. The real color variation is appreciable from the sedimentation process and after the drying process where the filtered solution appears transparently and lightly orange while the powder on the filter has an extremely deep dark red hue (Fig. 11–12).

Since the stoichiometric numbers for the complexation reaction are not precisely defined and just an approximate quantity of the two compounds is provided in literature the synthesis was conducted multiple times varying the reaction conditions to determine the most efficient ration between the two reagents. The Table 4 shows the different ratio used between the reagents:

Table 4. Precise quantities used in the eosin syntheses

	1 <sup>st</sup>	2 <sup>nd</sup>	3 <sup>rd</sup>
$m_{\text{Eo}}$ [g]	0.51	1.00	1.00
$m_{\text{Al}}$ [g]	1.62	7.84	16.24
ratio Al/Eo	3.17	7.82	16.25



Through appropriate techniques the suitable ratio is selected, as the following paragraphs are going to explain. The most efficient reaction set the proportion approximately to 1 : 8 for eosin Y : Aluminum chloride hexahydrate in grams.

A second approach was tried by using an aluminum chloride solution as a starting point. This methodology proved to be impractical from the outset as a basic environment facilitates the dissolution of eosin Y while disfavoring the aluminum salt dissolution phenomenon.

### 3.2. Madder

The synthesis of Madder Lake was conducted based on Lombardi recipe [31]. 15 g of madder chips (Kremer) (Fig 14) were soaked in 1125 ml of distilled water for 1 hour at 60°C degrees (Fig. 15–16). The wood was removed from the beaker by filtering it. A 75 ml solution of a 10% (w/w) of  $KAl(SO_4)_2$  (Sigma Aldrich) was prepared with an acid pH around 3 and it was added to the batch. The final solution was neutralized with an addition of a solution of  $K_2CO_3$  (Kremer) at 0,1 M. The solution rested for 12 hours (Fig. 17) and then the solid pigment was obtained throughout filtration (Fig. 18,20), drying (Fig. 21) and grinding (Fig. 22–23). The filtration was slowly carried out and the filtrate was washed away until the wash water remained colorless.



Figure 14. Madder lake roots chips



Figure 15. Madder lake initially soaking

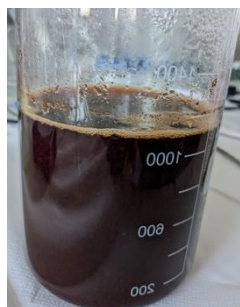


Figure 16. Madder lake after the soaking



Figure 17. Solution after the sedimentation



Figure 18. Filtration process



Figure 19. Paper filter during the filtration



Figure 20. Wet pigment

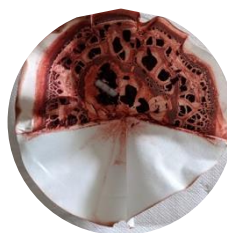


Figure 21. Dry pigment

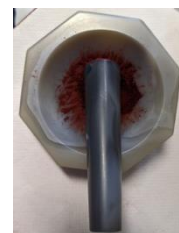


Figure 22. Grinding process



Figure 23. Final pigment

### 3.3. Brazilwood

The Brazilwood synthesis was based on the Jessie Wei-Hsuan Chen's recipes [32, 33]. The Brazilwood chips (Kremer)(Fig. 24) were weighted as 15g and then soaked in 250 ml in distilled water for 1h at room temperature (Fig. 25). Then the mixture was heated till the boiling point and let it boil under stirring for 10 min (Fig. 26). The wood was removed from the beaker through filtration. After the addition of 5g of alum(Sigma Aldrich), the dye solution was heated again to 80°C degrees and a solution of 12 g of gypsum (Kremer) in 100 ml of distilled water was added (Fig. 27). The filtration occurs after 12 hours of resting, the pigment was washed till the washing waters remain transparent (Fig. 28–29). The filtered pigment was allowed to dry completely before grinding manually (Fig. 30,32). The obtained pigment was stored protected from the light.



Figure 24. Brazilwood shavings



Figure 25. Brazilwood initial soaking



Figure 26. Heating the solution



Figure 27. Solution after the sedimentation



Figure 28. Filtration process



Figure 29. Paper filter during the filtration



Figure 30. Dry pigment



Figure 31. Grinding process



Figure 32. Final pigment

### 3.4. Cochineal

The pigment was not synthesized because of literature evidence, Geldof et al. pointed out how within Van Gogh's palette the cochineal used finds the greatest similarities with the commercial product proposed by Kremer[9]. The pigment used to create the samples was selected as the Carmine nacarot cochineal rot Kremer 42100.



### 3.5. Synthesis of lead white

The synthesis of hydro cerussite was conducted based on the studies of Gebeyehu and Boström [34]. A 1l solution of lead nitrate at 0,02M concentration was prepared (Fig. 33) and a 1l solution of sodium carbonate at 0,13M with an ammonia addition (Fig. 34) to obtain a basic environment (see Table 5). After the dissolution of the nitrate salt, the soft basic working conditions guarantee the stability of hydro cerussite formation instead of cerussite.

In order to speed up the dissolution of the lead nitrate solution heating was used for twenty minutes. When both the solutions appeared transparent, meaning the dissolution was complete, they were added simultaneously in a proper beaker to maintain in every moment an averaged and constant basic pH (Fig. 35). After one hour the obtained solution was filtered and dried for 24 hours. The obtained solid was grinded (Fig. 36) in a mortar and stored (Fig. 37). The total amount of the hydro cerussite obtained was around of 3,4 g. In order to obtain lead white 0,67 g of cerussite were added[35].

Table 5. Concentration parameter of the reaction.

	Lead Nitrate solution	Sodium Carbonate solution
m [g]	6.6540	1.3411
n [mol]	0.0201	0.0127
C [M]	0.0201	0.0127



Figure 33. Lead nitrate solution



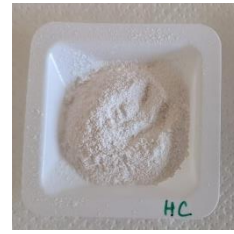
Figure 34. Sodium carbonate solution



Figure 35. Resulting solution during sedimentation



*Figure 36. Ground product*



*Figure 37. Final hydro cerussite*

## 4. Particle size evaluation

The materials obtained were ground manually in a mortar after drying the powders. Since the purpose of the research is to create oil painting models, it is important to document the characteristics of the materials used. Via microscopic observation (Nikon), it was possible to obtain an approximate assessment of the average particle size (Table 6). A small amount of powder was placed on the microscope slide and then homogeneously interspersed. During the focusing on a suitable sample portion, the instrument magnification was selected. Using the tools provided by the software, it was possible to take the approximate size of a large number of particles ( $n > 30$ ) and obtain the average size of the investigated sample (Fig. 38–39).

Table 6. Average particle sizes evaluation

	Average length [ $\mu\text{m}$ ]	Sample size
PbW	$1.7 \pm 1.3$	65
eosin	$2.3 \pm 1.3$	65



Figure 38. Lead white particles evaluation thanks to the software

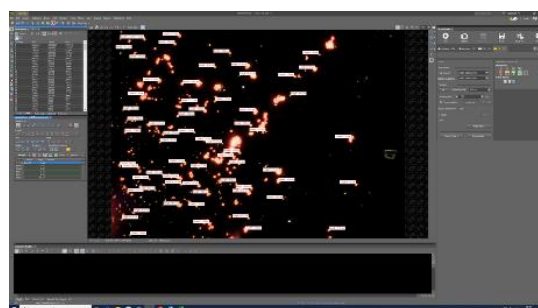


Figure 39. Eosin particles evaluation thanks to the software

The average pigment size is a parameter that influences the creation of oil painting. The ratio of surface area to volume increases as the volume decreases, thus increasing the wettability of the powder affecting the final resulting paint[36]. The following images show the appearances of the synthesized eosin pigment in its main agglomerates (Fig. 40–41).

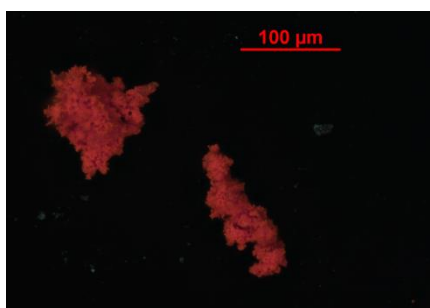


Figure 40. Eosin particles (10x magnification)

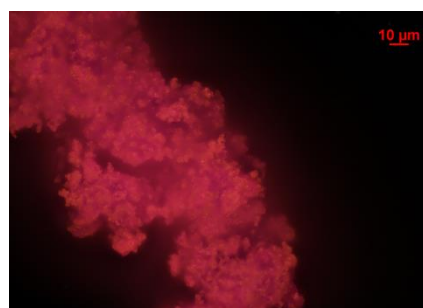


Figure 41. Eosin particles (50x magnification)

## 5. ATR-FTIR analysis of eosin

IR analyses conducted on the reaction products were compared with the starting reagent, eosin Y (Fig. 37). The characteristic signals of eosin Y can be summarized as follow:  $3470\text{ cm}^{-1}$  attributed to the hydroxyl group affected by the bromine in *ortho* position, xanthere rings' signals are between  $1616\text{--}1464\text{ cm}^{-1}$  and  $1750\text{ cm}^{-1}$ ,  $1210\text{ cm}^{-1}$  represent the lactone conformation [4, 13, 37]. The product spectra show the persistence of the same signals (grey areas), which is why it can be said that the reaction did not take place completely. The presence of eosin is demonstrated by the presence of the characteristic signals at  $1557\text{ cm}^{-1}$  and  $1435\text{ cm}^{-1}$  linked to the symmetrical and asymmetrical stretching of C=O (blue areas) [4, 38]. In the appendix all the spectra of eosin Y and the three different eosin produced are collected (Fig. 42) [39–41].

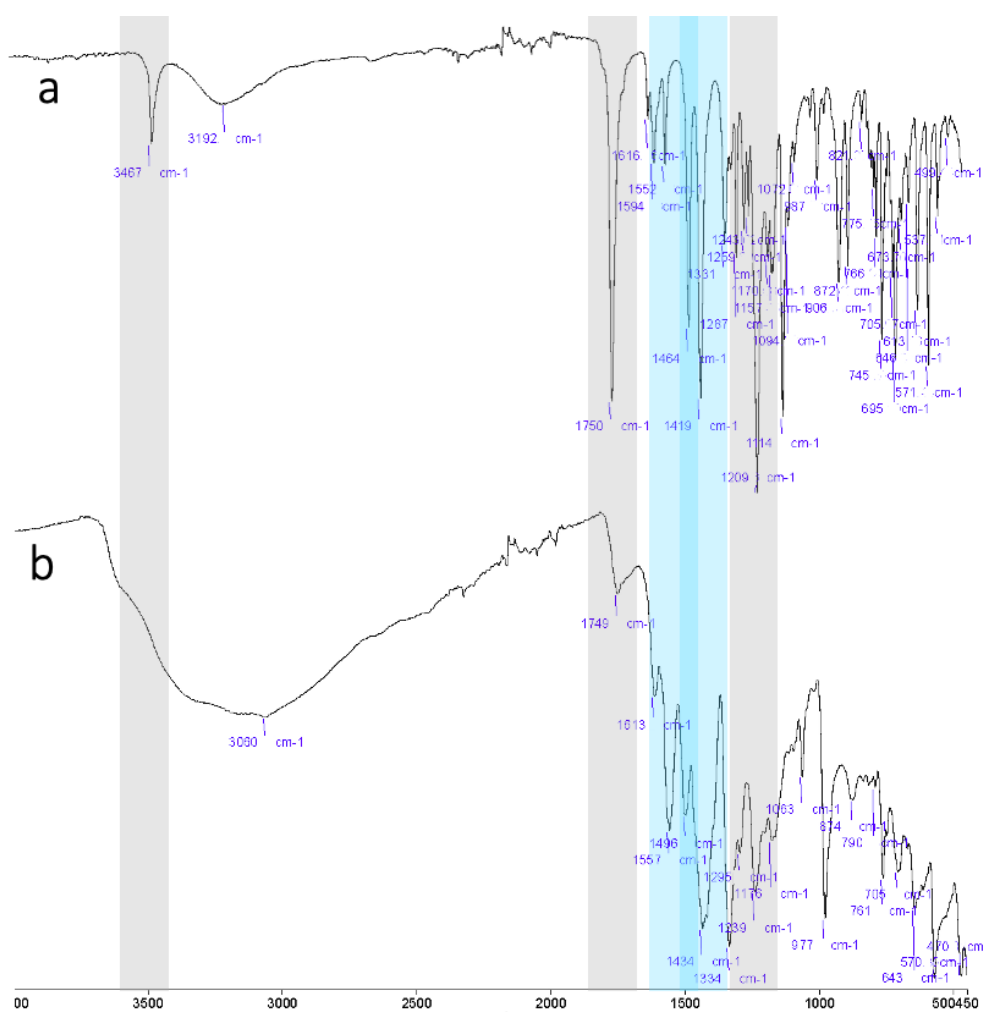


Figure 42. ATR-FTIR spectra of (a) eosin pigment and (b) eosin Y where grey areas represent the eosin Y characteristics peaks and blue areas the eosin complex's ones.

## 6. Molecular characterization by TOF-MS solvent optimization

The analysis of eosin synthesized in the laboratory was enriched by mass spectrometry. Compared to IR molecular spectroscopy, mass spectrometry is able to provide precise information about the  $m/z$  ratio of the chemical species present in the samples under investigation. Thus, it was possible to demonstrate the presence of the pigment of interest, the aluminum-eosin complex (Eo-Al-Eo,  $m/z=1318$ ) (Fig. 43-44) (Appendix Table 24) highlighted by the blue bands. All the eosins examined contain the alumina complex, so the discriminating factor in selecting the most suitable product was the presence or absence of secondary products.

As Figure 44 shows, the eosin obtained from the second synthesis contains not only the alumina complex, but at the same time the relative amount of by-products is lower compared to the three samples [2, 42-48].

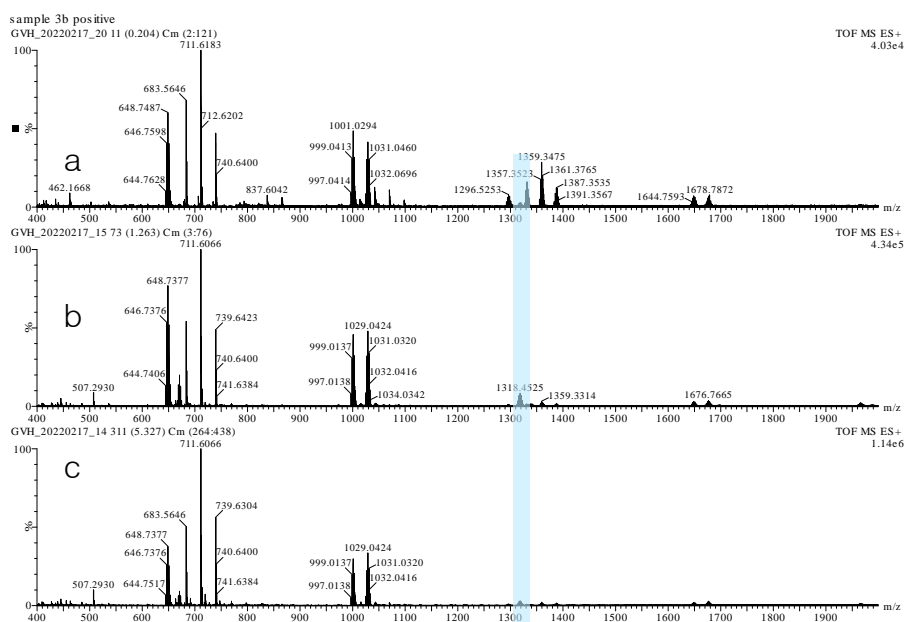


Figure 43. TOF-MS-ES+ spectra of eosin (a) firstly, (b) secondly and (c) thirdly synthesized where the blue area highlights the eosin-Al complex mass

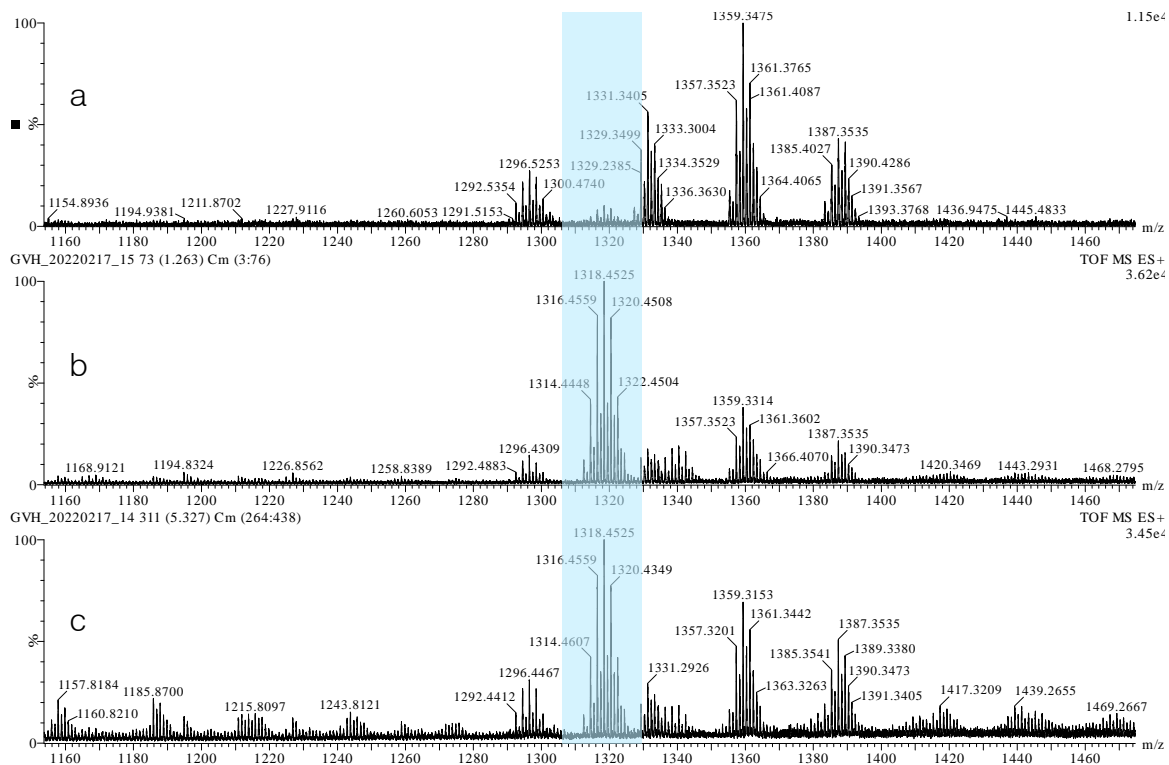


Figure 44. Magnification in the range 1150-1450 m/z of mass spectra of eosin (a) firstly, (b) secondly and (c) thirdly synthesized where the blue area highlights the eosin-Al complex mass

## 7. XRPD analysis for lead white

XRPD analysis enabled us to determine the purity of the product obtained during the synthesis and the lead different crystal structures content of the pigment thanks to Rietveld refinement through XRDUA software [17, 49]. The initial synthesis did not guarantee the purity that was expected (Table 7 and Figure 45–47–48), probably because a sufficiently basic pH condition was not ensured during the transfer of the solutions into the main beaker. In any case, the ratio of cerussite to hydro cerussite in the final pigment is consistent with the literature data [35] (Table 7 and Figure 46–47–48).

Table 7. XRPD results for lead powders

	HC [% wt]	C [% wt]
Hydro cerussite synthesized	29.7	70.3
Lead white	22.5	77.5

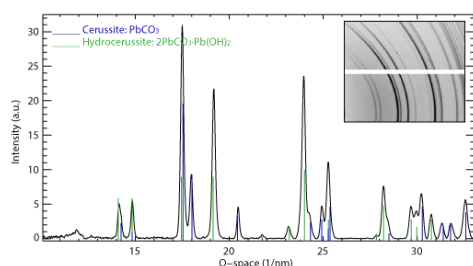


Figure 45. XRPD spectrum of hydro cerussite synthesized

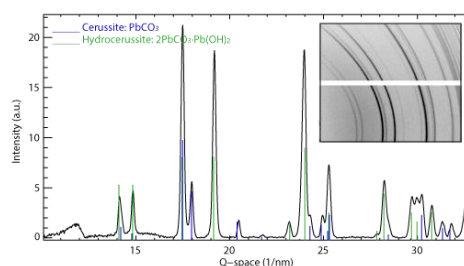


Figure 46. XRPD spectrum of lead white pigment

### Reference spectra

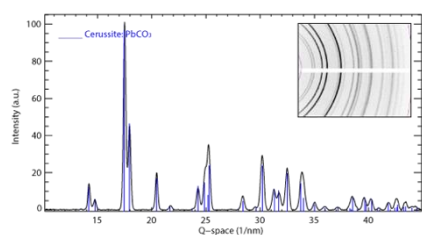


Figure 47. XRPD reference spectra of cerussite

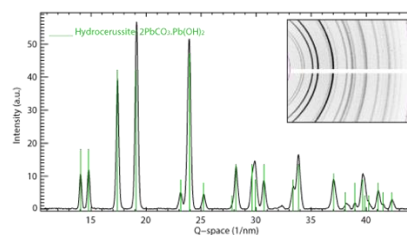


Figure 48. Reference spectra of hydro cerussite

## 8. Oil absorption value

Oil absorption is defined as the ratio of the amount of oil by weight needed to form a stiff but spreadable paste from a known quantity of pigment, and is usually expressed as the number of grams of oil needed for 100 grams of pigment[50].

As the use of eosin mainly took place within oil paintings, it was decided to work with a model that could be as close as possible to real examples, and so it was decided to create samples of linseed oil paintings.

In order to introduce a standardized methodology for the oil samples the Oil Absorption value (OA) was calculated starting from small amounts of pigments (Table 8)[51].



Knowing the linseed oil's drop average weight  $26,5 \pm 3,2$  mg, the poppyseeds oil's drop average weight  $28,0 \pm 2,4$  mg and knowing the amount of pigment used for each evaluation, the number of drops of oil that each one request to obtain a painting of the intended workable consistency was collected. The procedure was performed five times for each pigment.

Figure 49. OA evaluation in laboratory

Table 8. OA obtained values

Pigment	OA of Linseed Oil [g]	OA of Poppyseeds Oil [g]
HgS	$19.0 \pm 1.6$	$22.4 \pm 2.5$
CoB	$56.3 \pm 7.0$	$49.0 \pm 4.6$
PbW	$25.7 \pm 6.3$	$28.1 \pm 4.2$
ZnW	$29.4 \pm 7.4$	$26.0 \pm 6.8$
Eo	$92.1 \pm 9.4$	$80.0 \pm 14.3$
Coc	$95.9 \pm 6.6$	$87.7 \pm 5.0$

Working with larger amounts of pigment ( $>2$  g) increases the accuracy of the measurement. One is also aware that the process depends heavily on the operator's decisions. In the future, it is hoped that it will be possible to obtain results averaged over the evaluation of several operators in order to mediate the subjective error resulting from the addition decision.

## 9. Preparation of the oil paints

The pure oil paints were singularly composed for each pigment following the OA value and the right consistency by adding drop by drop the linseed oil. The second step was the creation of the mixtures by weight ratios (example: 1,9 g of A + 0,1 g of B). The following Table 9–10 are showing the obtained samples, resulting in six reference sample for the pure pigments, fifteen eosin-based samples and sixteen cochineal-based samples.

Table 9. Eosin-based samples

	eosin						0 : 100
	100 : 0	>99 : <1	99 : 1	95 : 5	50 : 50	5 : 95	
CoB	X			X	X	X	X
HgS	X			X	X	X	
PbW	X	X	X	X	X	X	
ZW	X	X		X	X	X	





Figure 50. Cobalt blue mixture samples



Figure 51. Vermilion mixture samples



Figure 52. Lead white mixture samples

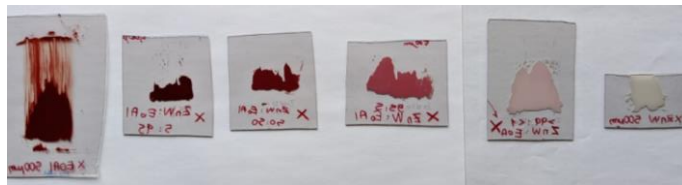


Figure 53. Zinc white mixture samples

Table 10. Cochineal-based samples

	Cochineal						0 : 100
	100 : 0	>99 : <1	99 : 1	95 : 5	50 : 50	5 : 95	
Cobalt Blue	X		X	X	X	X	X
Vermilion	X		X	X	X	X	
Lead white	X	X		X	X	X	
Zinc white	X	X		X	X	X	

The set-up for the drying process is illustrated in the Figure 54. The samples were allowed to dry in the dark for 20 days, the samples were housed inside a structure covered with aluminum foil that allows the absence of light but the entry of air and oxygen, which is essential for the drying of the oil process. Once the surface of all samples was dry-to-touch, the samples were placed all together at the same time in front of a west-facing window subjected to a broad spectrum of light irradiation from the sun partially shielded by glass (Fig. 55)[43].

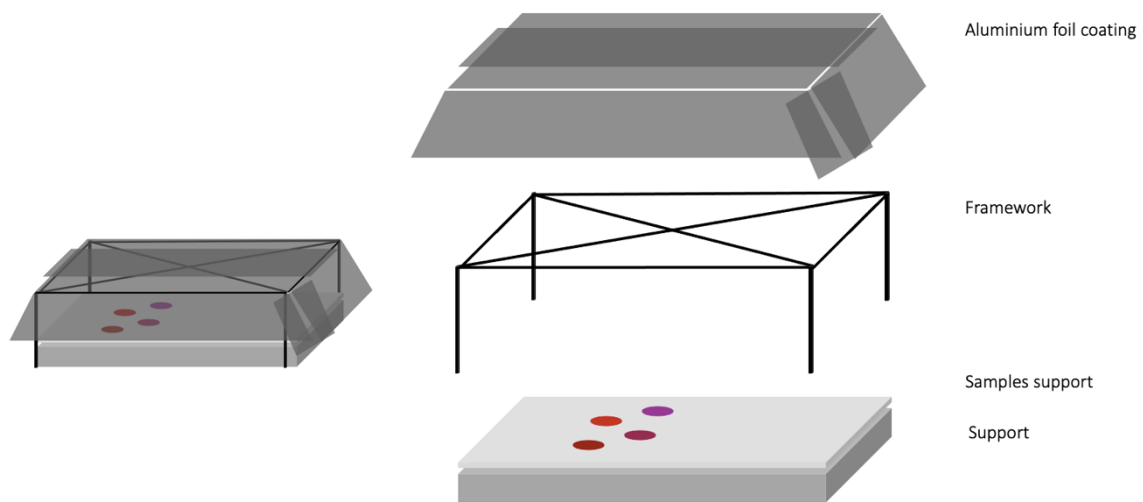


Figure 54. Drying set-up scheme

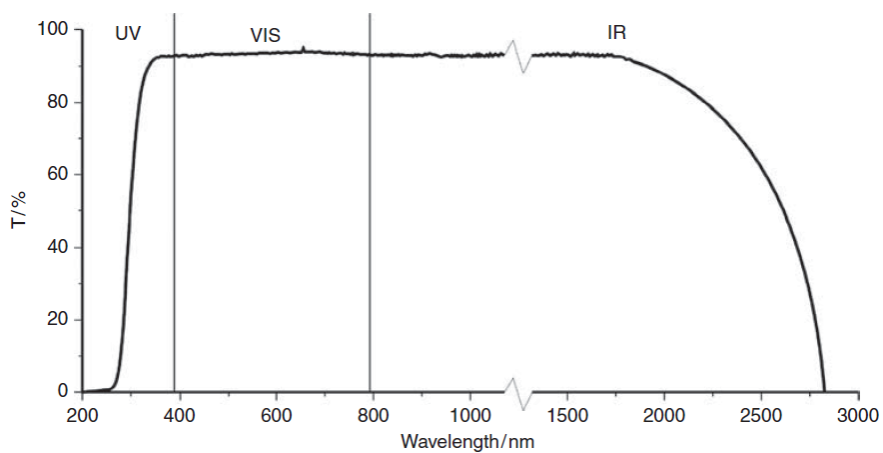


Figure 55. Optical absorption spectrum from a conventional colorless soda-lime glass

For a period of about 107 days, the samples were left to age in front of the window and their reflectance spectra and colorimetric coordinates in CIELAB color space were periodically collected using FORS.

## 10. Monitoring total color change: data analysis

The data obtained through FORS, and colorimetry were statistically treated thanks to R language and Rstudio software each mixture between eosin and the inorganic pigment selected. The FORS spectra collected during the 40 days of aging show the coherent, showing the eosin the flexion at 620 nm while cobalt blue is absorbing in the range between 550 and 650 nm (Fig. 56,60).

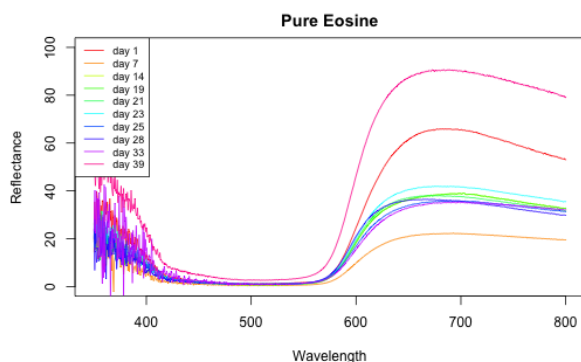


Figure 56. eosin FORS spectra during the aging

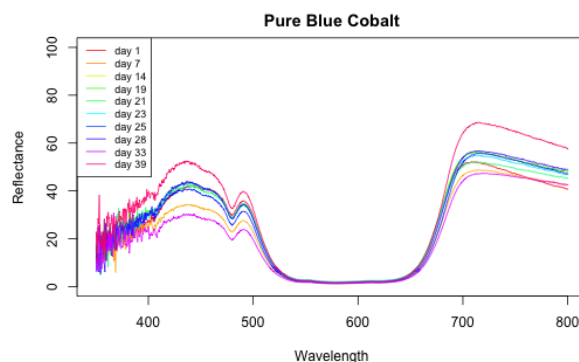


Figure 57. cobalt blue FORS spectra during the aging

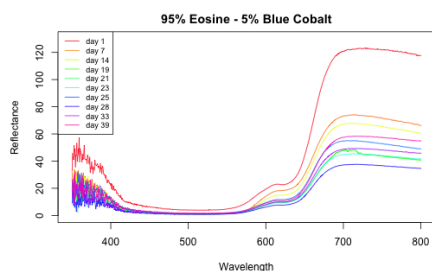


Figure 58. 95% eosin FORS spectra during the aging

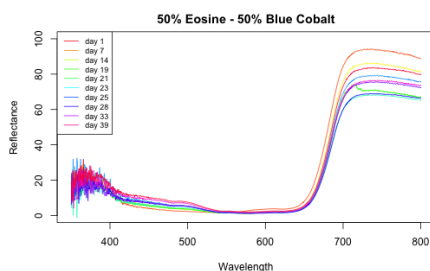


Figure 59. 50% eosin FORS spectra during aging

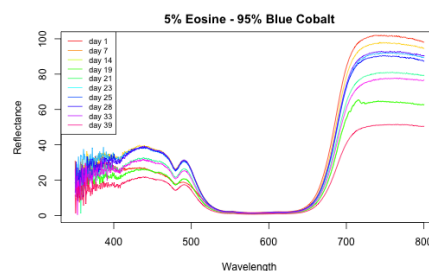


Figure 60. 5% eosin FORS spectra during the aging

The Rstudio software allowed us to illustrate the colorimetric data of the entire dataset of samples over time in L\*a\*b\* space, as depicted in Figure 61. Thanks to the following histograms (Table 11) is possible to visualize the color variation that affects the samples in 40 days.

## Colorimetric data of the Cobalt blue mixtures

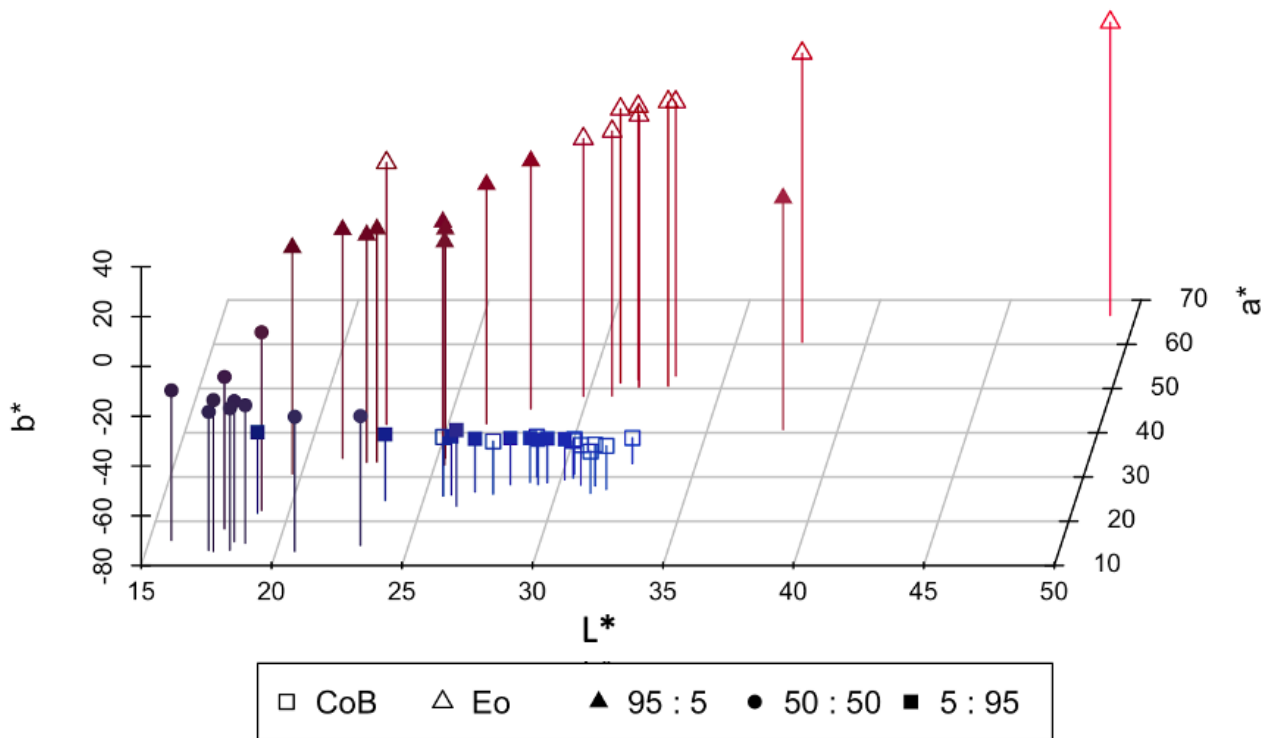


Figure 61.  $L^*a^*b^*$  tridimensional representation of the samples

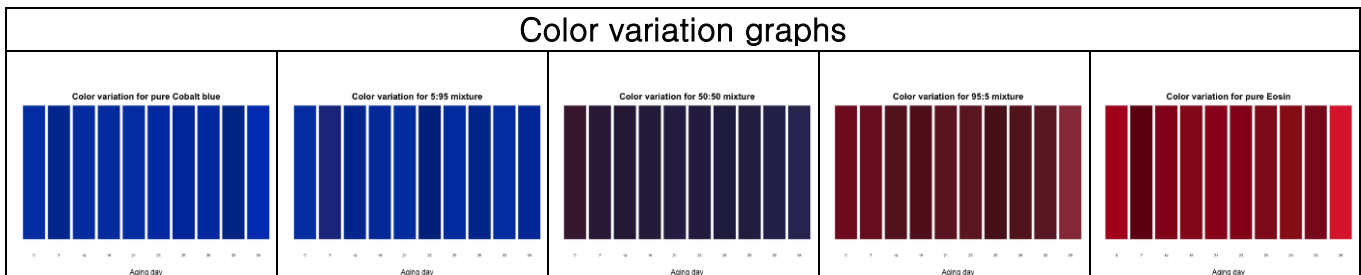


Table 11. Table of histograms of color variation during the time

Starting from the illustration of the FORS spectra collected over time, it was possible to calculate the cluster analysis for the dataset selecting the Euclidean distance and the Ward's method considered the most widely used of the hierarchical agglomerative method. The dendrogram (Fig. 62) defines three main groups based of the FORS spectra: the high eosin percentage group (100% and 95% content of eosin); the cobalt blue group (0% content of eosin) and the lower percentage group (50% and 5% content of eosin).

## Cobalt blue and Eosin mixture cluster analysis

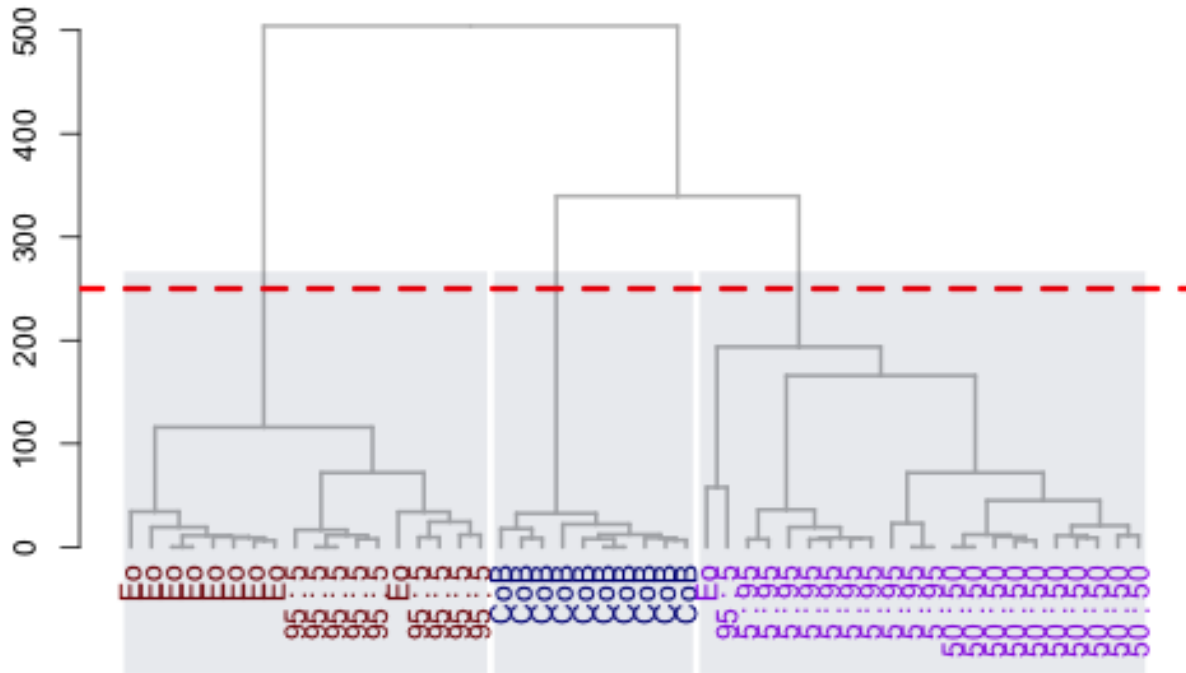


Figure 62. Dendrogram of eosin and cobalt blue samples

The principal components analysis was performed on the dataset since the cumulative variance was higher than 94% for three components (Fig. 63). The loadings plots explain that the main importance signals are the one related to eosin and cobalt blue characteristics ranges and their flexions (Fig. 64,66). On the biplot graphs the clusters are appreciable, especially on the first principal component, the results as expected are coherent with cluster analysis (Fig. 67,69). On all the samples the analyses were run and just an example is reported here to illustrate the outputs of the analyses. It is hoped that further future studies will help reveal new correlations between the color variation and the ageing time the samples were subjected to.

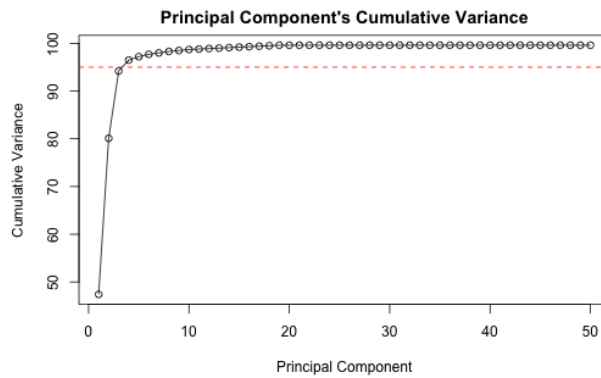


Figure 63. Cumulative variance plot

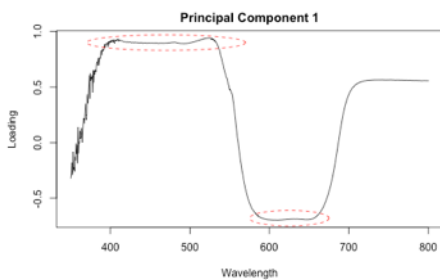


Figure 64. Loading plot for the first principal component

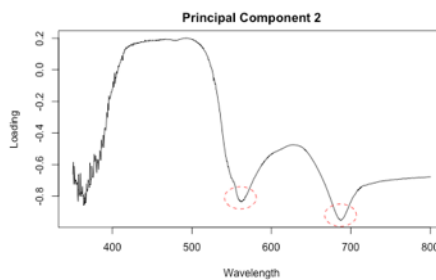


Figure 65. Loadings plot for the second principal component

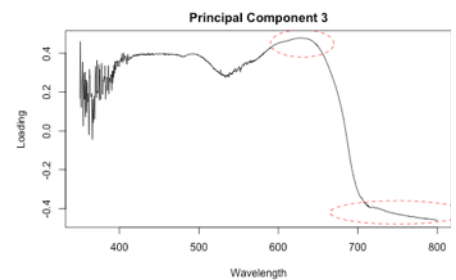
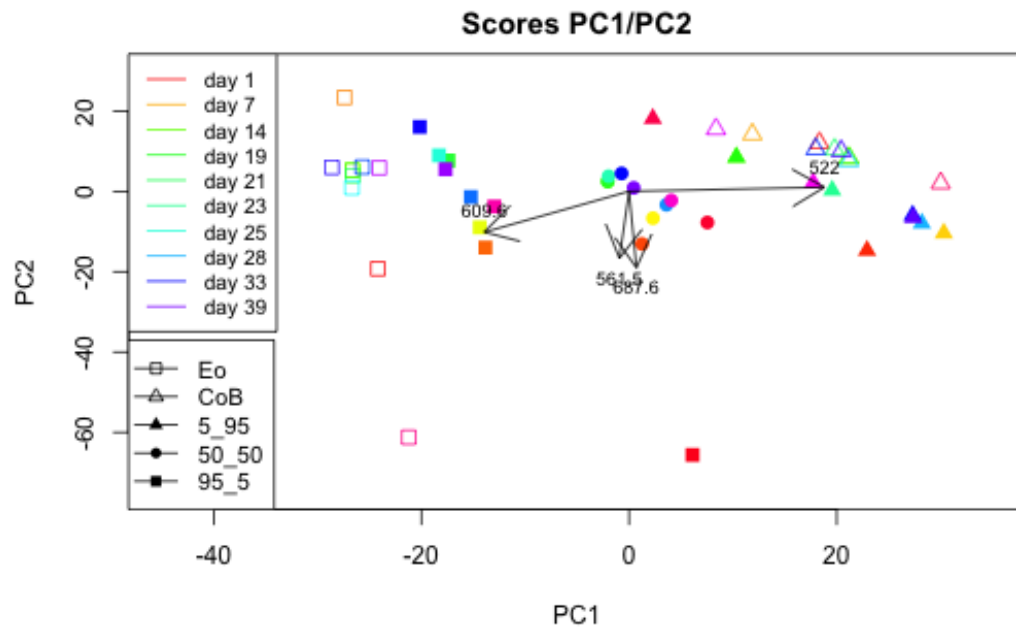
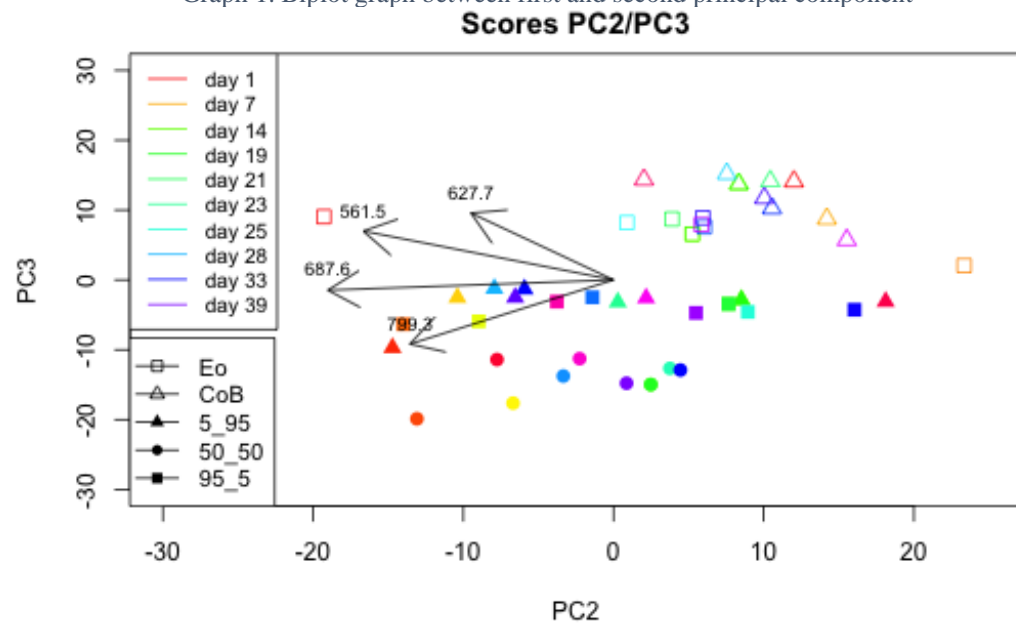


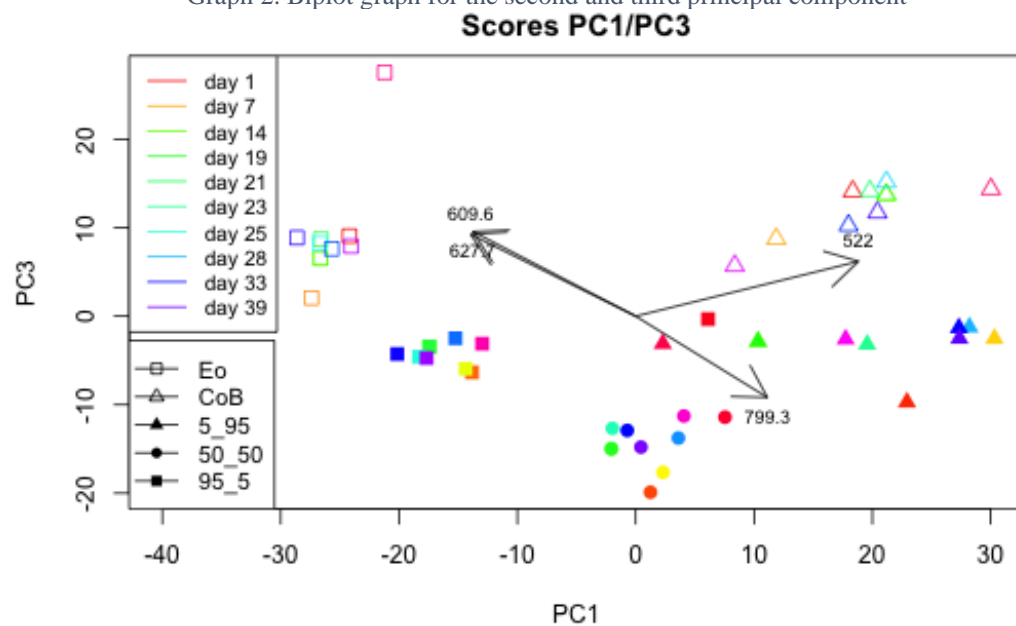
Figure 66. Loadings plot for the third principal component



Graph 1. Biplot graph between first and second principal component



Graph 2. Biplot graph for the second and third principal component


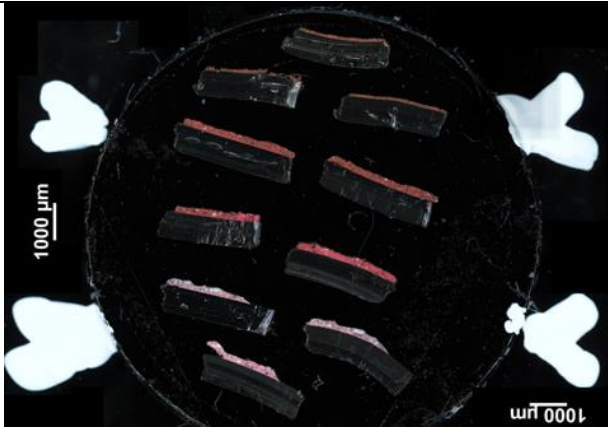



Graph 3. Biplot graph for the first and third component

## 11. MALDI-MSI samples

The images of all analyzed samples are shown in the following Tables 12–13 using two different optimal performance tapes. For each tape, all different concentration samples referring to the same degree of ageing were placed in. Two or more replicas were collected for each concentration sample.

Table 12. Analyzed sample resume

	Sample on Carbon tape	oil paint combination with PbW
0 days of aging		<p>100% eosin – 2 thin sections</p> <p>95% eosin – 2 thin sections</p> <p>50% eosin – 2 thin sections and a fragment</p> <p>5% eosin – 2 thin sections</p>
7 day of aging		<p>100% eosin – 3 thin sections</p> <p>95% eosin – 2 thin sections</p> <p>50% eosin – 2 thin sections</p> <p>5% eosin – 3 thin sections</p>
40 days of aging		<p>100% eosin – 3 thin sections</p> <p>95% eosin – 2 thin sections</p> <p>50% eosin – 2 thin sections</p> <p>5% eosin – 2 thin sections</p>





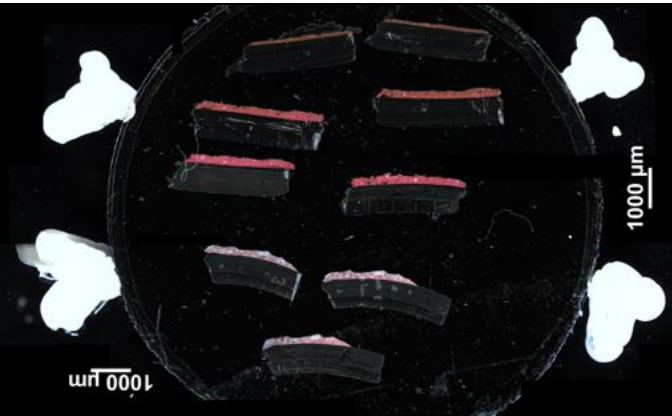
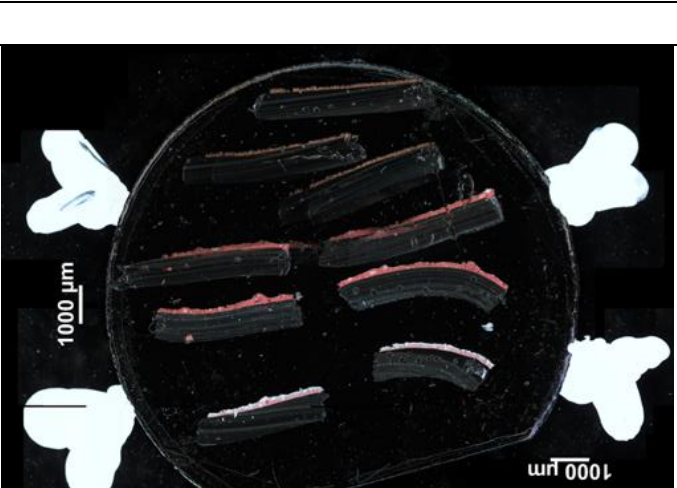
107 days of aging		<p>100% eosin – 3 thin sections</p> <p>95% eosin – 2 thin sections</p> <p>50% eosin – 2 thin sections</p> <p>5% eosin – 2 thin sections</p>
-------------------	--	---

Table 13. Analyzed samples

oil paint combination with PbW	Sample on Carbon tape Al-core	
<p>100% eosin – 2 thin sections</p> <p>95% eosin – 2 thin sections</p> <p>50% eosin – 3 thin sections</p> <p>5% eosin – 2 thin sections</p>		0 days of aging
<p>100% eosin – 2 thin sections</p> <p>95% eosin – 2 thin sections</p> <p>50% eosin – 2 thin sections</p> <p>5% eosin – 2 thin sections</p>		7 day of aging



<p>100% eosin – 3 thin sections</p> <p>95% eosin – 2 thin sections</p> <p>50% eosin – 2 thin sections</p> <p>5% eosin – 2 thin sections</p>		<p>40 days of aging</p>
<p>100% eosin – 3 thin sections</p> <p>95% eosin – 2 thin sections</p> <p>50% eosin – 2 thin sections</p> <p>5% eosin – 2 thin sections</p>		<p>107 days of aging</p>

## 12. MALDI-MSI analyses

### 12.1. Results

The results in the Table 14 quantified the amount of eosin in each sample over time. If the chromophore moiety part is still present, the color may remain intact, which is why we first check the permanence of the eosin molecule. The loss of eosin is stronger in the samples with a high concentration of lead white, suggesting that its presence may be involved in the degradation process path[46] while in the 100% eosin samples its concentration increases till the 40<sup>th</sup> day and slowly decreases after. Debromination is considered the first step in the degradation process of the pigment. Table 15 allows to visualize the distribution of the eosin molecule in the sample series and contemporary to visualize the distribution of the debrominated product[52].

Table 14. Results of eosin content in the samples

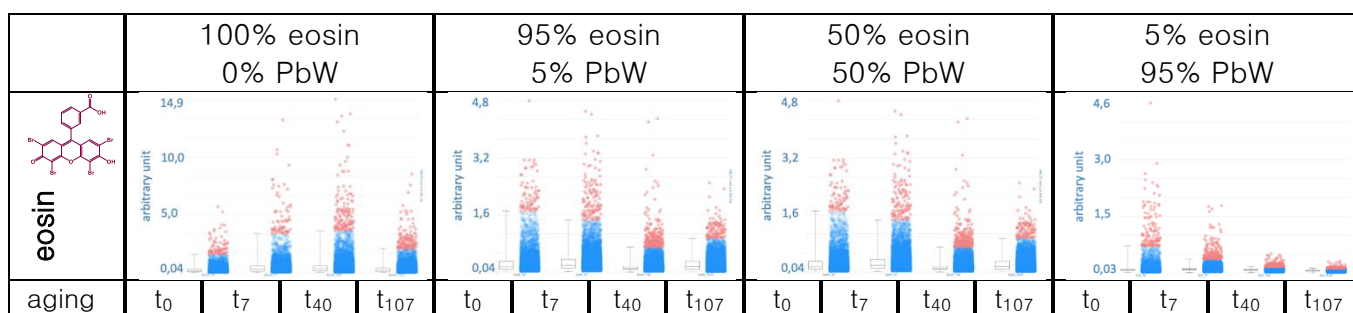


Table 15. Distribution maps of eosin and debrominated eosin over samples aged 7 days

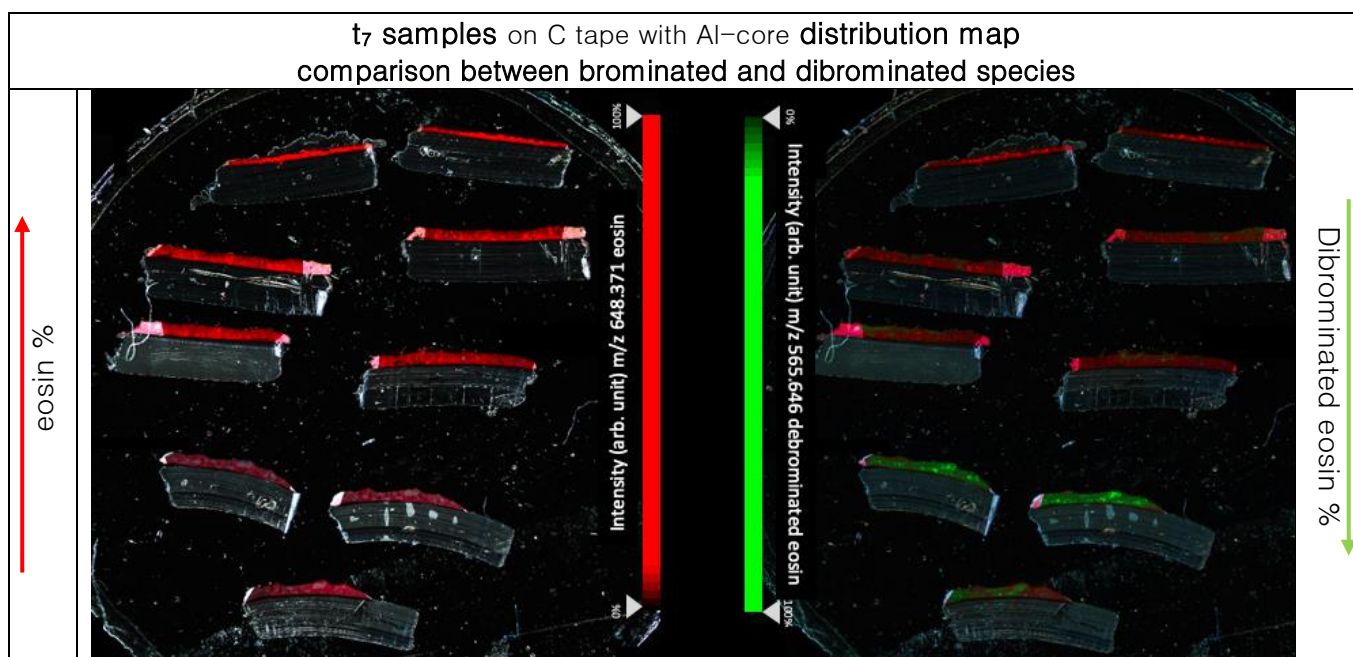


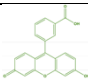
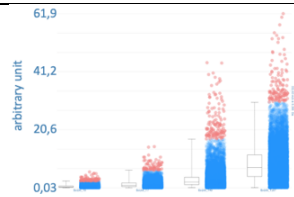

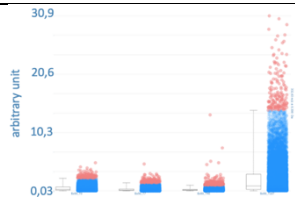
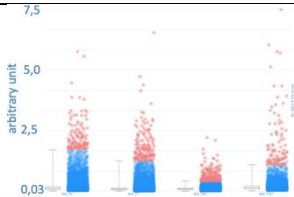
Table 16 makes it easy to read the results by comparing the microscopic image (a, d, g, l) with the distribution of eosin (red) (b, e, h, m) and the distribution of the debrominated species (green) (c, f, i, n) for all samples with different eosin concentrations aged 7 days. It is possible to find matches within the pictorial layers between the eosin distributions and the microscopic image. First of all, the eosin map (b) in the 100% eosin pictorial layer is the most intense of the group, whereas the map (m) of the 5% eosin sample is a faint red with some small intense areas representing pigment grains, poorly amalgamated in the paint. The distribution map of the debrominated species is further interesting. It can be said that within the (c) 100% eosin sample is almost completely absent as no green signal is visible. The (d) 95% and (e) 50% samples show a similar situation, although more evident in the second section. The presence of the bromine-free specie is predominant in the areas around the paint surface or where there are cracks in the paint while the grains of eosin are still visible in the lower areas. The sample with the lowest concentration of eosin shows the highest concentration of by-products, distributed almost homogeneously within the paint layer. In particular in particular at the main grains of lead white (l) the most intense signals of the map (i) are found.

Table 16. Comparison between eosin and debrominated eosin distribution focusing individually on each section

samples t <sub>7</sub>			
	microscopic image	eosin distribution map	debrominated eosin distribution map
	<b>1000 μm</b>	Intensity (arb. unit) m/z 648.371 eosin	Intensity (arb. unit) m/z 565.646 debrominated eosin
	a	b	c
100 % eosin			
	d	e	f
95 % eosin			
	g	h	i
50 % eosin			
	l	m	n
5 % eosin			

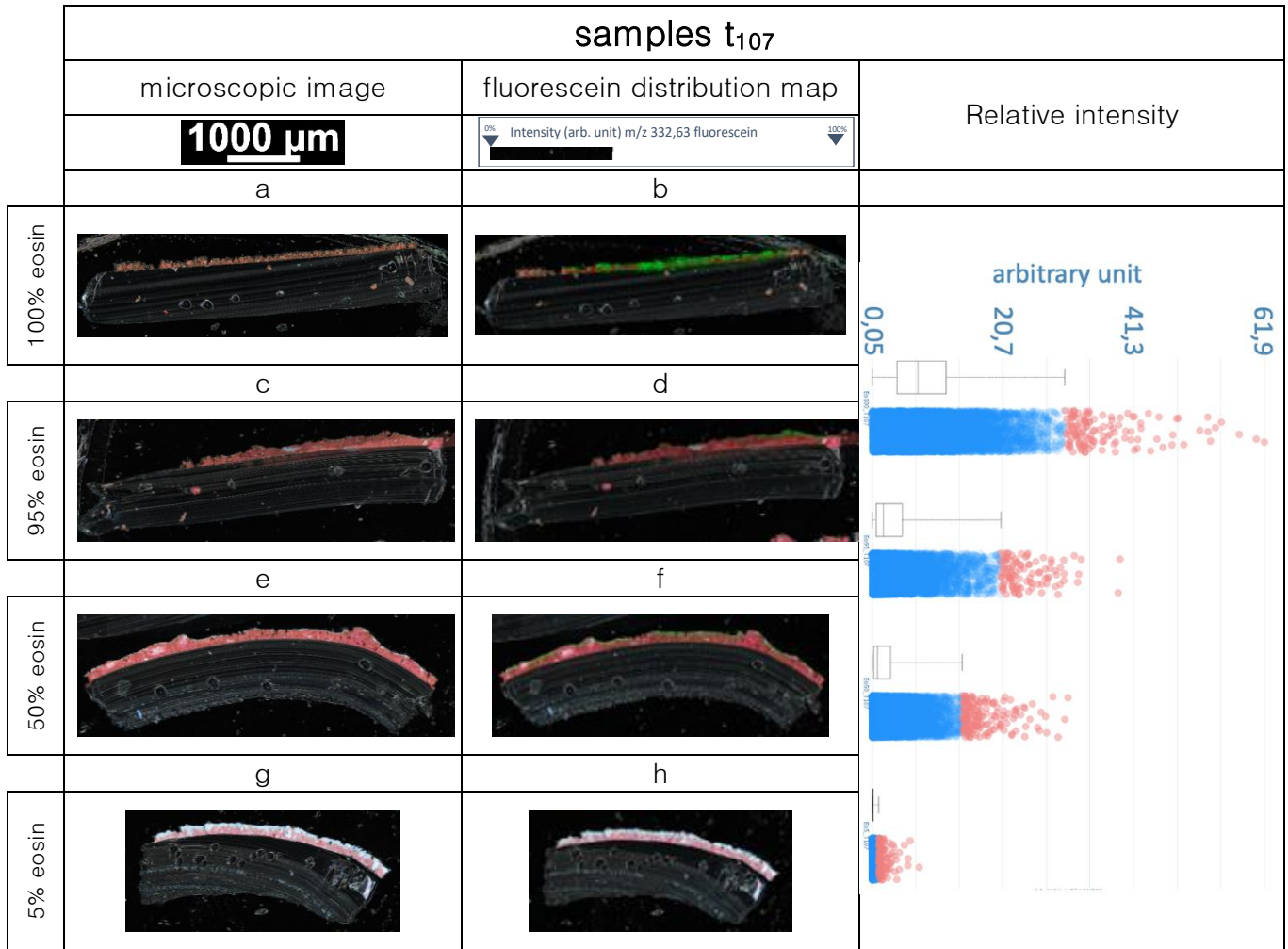
Fluorescein distribution is interesting to monitor, as it is composed by the same carbon skeleton of eosin, without the bromines, and therefore can be considered the product of the complete debromination process. In all the analyzed cases fluorescein is present in the unaged samples, but its concentration is increasing over time. Where the lead white is absent, 100% eosin, as the Table 17 is resuming, the final amount of fluorescein is drastically higher.

Table 17. Results relative to fluorescein

	100% eosin 0% PbW	95% eosin 5% PbW	50% eosin 50% PbW	5% eosin 95% PbW
				
aging	t <sub>0</sub> t <sub>7</sub> t <sub>40</sub> t <sub>107</sub>	t <sub>0</sub> t <sub>7</sub> t <sub>40</sub> t <sub>107</sub>	t <sub>0</sub> t <sub>7</sub> t <sub>40</sub> t <sub>107</sub>	t <sub>0</sub> t <sub>7</sub> t <sub>40</sub> t <sub>107</sub>

The Table 18 again compares the microscopic image of the samples with the distribution of the test species, fluorescein. The test samples were all aged 107 days, indeed from looking at the microscopic images it can be seen that specimen (g) has two overlapping layers, one pink and one white. It can be deduced that the white layer is an effect of the fading of the pigment under examination. Similarly, sample (e) has a much thinner layer. It can be seen that there is a consistent, thin, concentrated surface coating of fluorescein within the samples (d) 95% and especially (f) 50% eosin. The sample consisting entirely of eosin (b) shows fluorescein at all depths, also due to the thinness of the sample, while sample (f) with a low eosin content shows no detectable fluorescein concentrations

Table 18. Fluorescein distribution map over sample aged 107 days



One of the most interesting potentialities of MALDI-MSI consists in the map distribution of different molecules with high resolution and sensitivity. The following maps show the presence of two different degradation species coming from the asymmetrical breaking of the central oxacyclohexane ring and recombination of carboxylic groups[53]. The two compounds differ by a methyl group so around 16 Daltons. Thanks to this technique it is possible to obtain the mass spectrum of each point of the analyzed sample. Then, selecting the molecular weights of interest, it is possible to obtain different informative maps of each one singularly and also overlapping different distribution maps to obtain richer and more complex information. In this specific case the evidences allow to hypothesized that the two species are correlated as they are present in the same areas of the sample.

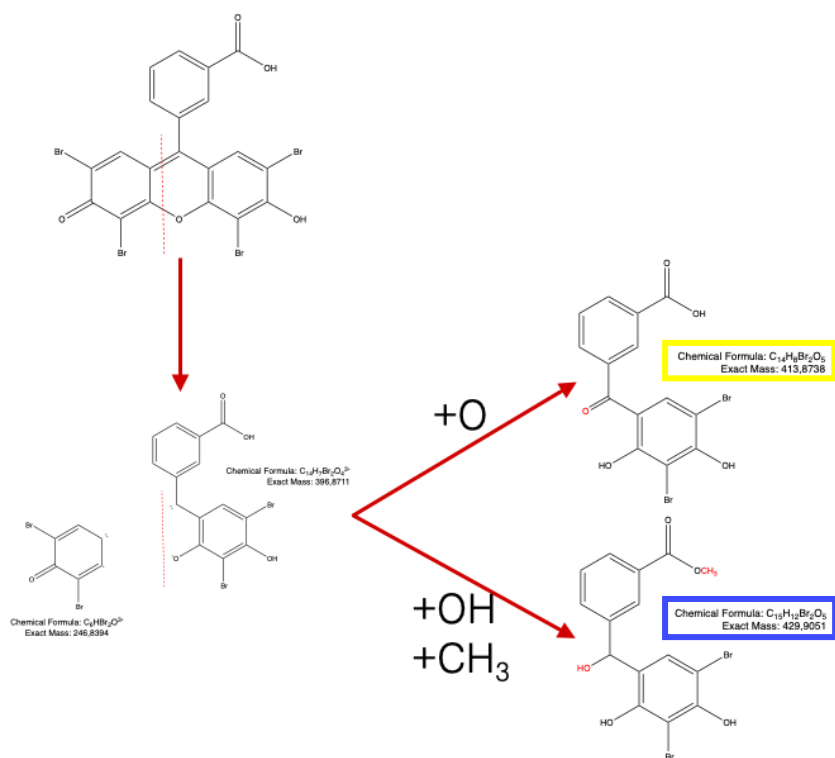
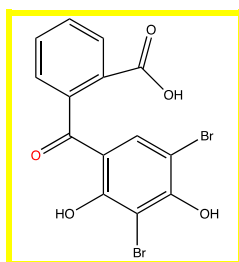


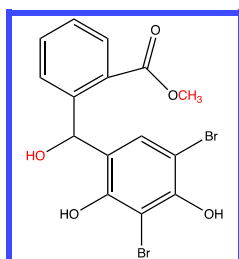
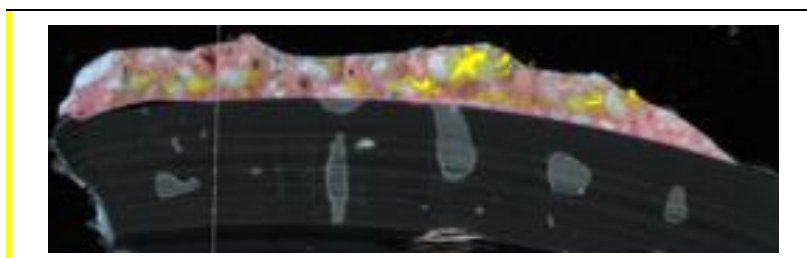
Figure 67. Tentative of the fragmentation process of the investigated molecules

Analyses of already aged samples are desirable in order to increase knowledge regarding pigment behavior in the presence of an oily binder and how the co-presence of different pigments can influence stability.





m/z 413,493



m/z 429,435



## 12.2. Discussion

The potential of this technique has been illustrated in the previous section. The possibility of obtaining mass spectrometric imaging of the organic fraction represents an innovation in the field of cultural heritage. The sample dimensions required are contained (10  $\mu\text{m}$  thickness). Furthermore, it does not require chemical pre-treatment such as extraction, purification, or separation of the components but a deposition or sublimation of the matrix. Information on imaging data is a big gain in descriptive terms. Following a pre-study of the target molecules, it is possible to choose a selection of masses to map their distribution across the multi-layered sample.

### 13. Future prospective

As far as future research goals are concerned, further research into the reproducibility of samples can be mentioned.

Knowing the Critical Pigment Volume Concentration (CPVC). It represents the minimum amount of oil needed to make a standard amount of pigment into a lean paint, with every pigment fully coated and all the spaces in between the pigment particles filled, leaving no voids. given the time-consuming procedure for measuring the density of each pigment and the demand for a large supply of material, it was decided to reserve the obtaining of CPVC for future research.

Analyses of already aged samples are desirable in order to enhance the knowledge regarding pigment behavior in the presence of an oily binder and how the co-presence of different pigments can influence its stability.

The applications of MALDI-MSI within the field of heritage science can be many. The study of drying oils and many other synthetic and natural organic molecules can be studied.



## 14. REFERENCES

1. Cooksey, C.J., *Quirks of dye nomenclature. 10. Eosin Y and its close relatives*. Biotech Histochem, 2018. **93**(3): p. 211-219.
2. Gosetti, F., et al., *Ultra-high-performance liquid chromatography/tandem high-resolution mass spectrometry analysis of sixteen red beverages containing carminic acid: identification of degradation products by using principal component analysis/discriminant analysis*. Food Chem, 2015. **167**: p. 454-62.
3. Zhang, F., et al., *Controlling Adsorption Structure of Eosin Y Dye on Nanocrystalline TiO<sub>2</sub> Films for Improved Photovoltaic Performances*. The Journal of Physical Chemistry C, 2013. **117**(28): p. 14659-14666.
4. Anselmi, C., et al., *Beyond the color: A structural insight to eosin-based lakes*. Dyes and Pigments, 2017. **140**: p. 297-311.
5. Dooley, K.A., et al., *Molecular Fluorescence Imaging Spectroscopy for Mapping Low Concentrations of Red Lake Pigments: Van Gogh's Painting The Olive Orchard*. Angew Chem Int Ed Engl, 2020. **59**(15): p. 6046-6053.
6. Centeno, S.A., et al., *Van Gogh's Irises and Roses: the contribution of chemical analyses and imaging to the assessment of color changes in the red lake pigments*. Heritage Science, 2017. **5**(1).  
September 24 2022]; Available from:  
<https://vangoghletters.org/vg/letters/let595/letter.html#original>.
7. Claro, A., et al., *Identification of red colorants in van Gogh paintings and ancient Andean textiles by microspectrofluorimetry*. Journal of Cultural Heritage, 2010. **11**(1): p. 27-34.
8. Geldof, M., et al., *Reconstructing Van Gogh's palette to determine the optical characteristics of his paints*. Heritage Science, 2018. **6**(1).
9. Ella Hendriks, L.J., Johanna Salvant, Élisabeth Ravaud, Myriam Eveno,, I.F. Michel Menu, Muriel Geldof, Luc Megens, Maarten van Bommel,, and C.R.J.J.a.D.H. Johnson, *A comparative study of Vincent van Gogh 's Bedroom series*, in *The National Gallery Technical Bulletin 30th Anniversary Conference Post prints*, Archetype, M. Menu, Editor. 2011. p. 237-43.
10. Alvarez-Martin, A., et al., *Photodegradation mechanisms and kinetics of Eosin-Y in oxic and anoxic conditions*. Dyes and Pigments, 2017. **145**: p. 376-384.
11. Doherty, B., et al., *Identifying Brazilwood's Marker Component, Urolithin C, in Historical Textiles by Surface-Enhanced Raman Spectroscopy*. Heritage, 2021. **4**(3): p. 1415-1428.
12. McHedlov-Petrossyan, N.O., et al., *2,4,5,7-Tetranitrofluorescein in solutions: novel type of tautomerism in hydroxyxanthene series as detected by various spectral methods*. Spectrochim Acta A Mol Biomol Spectrosc, 2005. **61**(11-12): p. 2747-60.
13. Claro, A., et al., *The use of microspectrofluorimetry for the characterization of lake pigments*. Talanta, 2008. **74**(4): p. 922-9.
14. Degano, I. and J. La Nasa, *Trends in High Performance Liquid Chromatography for Cultural Heritage*. Top Curr Chem (Cham), 2016. **374**(2): p. 20.
15. Degano, I., et al., *HPLC-DAD and HPLC-ESI-Q-ToF characterisation of early 20th century lake and organic pigments from Lefranc archives*. Heritage Science, 2017. **5**(1).
16. De Nolf, W., F. Vanmeert, and K. Janssens, *XRDU: crystalline phase distribution maps by two-dimensional scanning and tomographic (micro) X-ray powder diffraction*. Journal of Applied Crystallography, 2014. **47**(3): p. 1107-1117.
17. Cornett, D.S., et al., *MALDI imaging mass spectrometry: molecular snapshots of biochemical systems*. Nat Methods, 2007. **4**(10): p. 828-33.
18. Zaima, N., et al., *Matrix-assisted laser desorption/ionization imaging mass spectrometry*. Int J Mol Sci, 2010. **11**(12): p. 5040-55.
19. Hanrieder, J., et al., *Imaging mass spectrometry in neuroscience*. ACS Chem Neurosci, 2013. **4**(5): p. 666-79.

21. Marko Mank, B.S., and Günther Boehm, *2,5-Dihydroxybenzoic Acid Butylamine and Other Ionic Liquid Matrixes for Enhanced MALDI-MS Analysis of Biomolecules*. Analytical Chemistry, 2004. **76**, No 10.
22. Kramell, A.E., et al., *Mapping Natural Dyes in Archeological Textiles by Imaging Mass Spectrometry*. Sci Rep, 2019. **9**(1): p. 2331.
23. Tsang, J.-s., E. Friedberg, and T. Lam, *An easy-to-use method for preparing paint cross sections*. Journal of the American Institute for Conservation, 2019. **58**(3): p. 123-131.
24. Michele Derrick, L.S., Tanya Kieslich, Henry Florsheim, Dusan Stulik, *Embedding paint cross-section samples in polyester resins: problems and solutions*. Journal of the America Institute for Conservation, 1994. **33-3-1**: p. 227-245.
25. Sandu, I.C., et al., *Cross-section and staining-based techniques for investigating organic materials in painted and polychrome works of art: a review*. Microsc Microanal, 2012. **18**(4): p. 860-75.
26. Pouyet, E., et al., *Preparation of thin-sections of painting fragments: classical and innovative strategies*. Anal Chim Acta, 2014. **822**: p. 51-9.
27. Michael C. Fitzgerald, G.R.P., Lloyd M. Smith, *Basic Matrices for the Matrix-Assisted Laser Desorption/Ionization Mass Spectrometry of Proteins and Oligonucleotides*. Analytical Chemistry, 1993. **65**: p. 3204-3211.
28. Josiah C. McMillen, J.A.F., Dustin R. Klein, Jeffrey M. Spraggins, Richard M. Caprioli, *Effect of MALDI Matrices on Lipid Analyses of Biological Tissues using MALDI-2 Post-Ionization Mass Spectrometry*. ChemRxiv. Cambridge: Cambridge Open Engage, 2020.
29. S.G. Boxer, M.L.K., P.K. Weber, *Advances in Imaging Secondary Ion Mass Spectrometry for Biological Samples*. 2008.
30. Hankin, J.A., R.M. Barkley, and R.C. Murphy, *Sublimation as a method of matrix application for mass spectrometric imaging*. J Am Soc Mass Spectrom, 2007. **18**(9): p. 1646-52.
31. Lombardi, L., et al., *A new approach to the mild extraction of madder dyes from lake and textile*. Microchemical Journal, 2016. **126**: p. 373-380.
32. Chen, J.W.-H., *Planting Pigments ColLAB*.
33. Chen, J.W.-H., <Planting Pigments, Painting Plants>, in *An Exploration of Historical Experimental Plant-Based Lakes Pigments*. 2021.
34. Gebeyehu, M. and K. Boström, *The synthesis of hydrocerussite*. Geologiska Föreningen i Stockholm Förhandlingar, 1988. **110**(1): p. 67-68.
35. E. Welcomme, P.W., P. Bleuet, J.-L. Hodeau, E. Dooryhee, P. Martinetto, M. Menu, *Classification of lead white pigments using synchrotron radiation micro X-ray diffraction*. Applied Physics A, Material Science & Processing, 2007. **89**: p. 825/832.
36. Gueli, A.M., et al., *Effect of particle size on pigments colour*. Color Research & Application, 2017. **42**(2): p. 236-243.
37. Beltran, V., et al., *Geranium lake pigments: The role of the synthesis on the structure and composition*. Dyes and Pigments, 2021. **189**.
38. George, S., *Infrared and Raman characteristic group frequencies: tables and charts* W. Sons, Editor. 2001. p. 98.
39. Bellamy, L.J., *The Infrared Spectra of Complex Molecules*. Third edition ed. 1975.
40. Michele R. Derrick, D.S., James M. Landry, *Infrared Spectroscopy in Conservation Science*. Scientific tools for conservation. 1999.
41. Lili Wang, A.R., C. Meuse, A.K. Gaigalas, *Raman and FTIR spectroscopies of fluorescein in solutions*. Spectrochimica, 2001. **57**: p. 1781-1791.
42. Dapson, R.W., *The history, chemistry and modes of action of carmine and related dyes*. Biotech Histochem, 2007. **82**(4-5): p. 173-87.
43. Vargas, H.V., *Study of the aging of binders in proteinaceous media by high performance liquid chromatography*. 2008.
44. Lech, K., et al., *Identification of unknown colorants in pre-Columbian textiles dyed with American cochineal (Dactylopius coccus Costa) using high-performance liquid chromatography and tandem mass spectrometry*. Anal Bioanal Chem, 2015. **407**(3): p. 855-67.
45. Sabatini, F., et al., *The issue of eosin fading: A combined spectroscopic and mass spectrometric approach applied to historical lakes*. Dyes and Pigments, 2020. **180**.

46. Alvarez-Martin, A., et al., *Rapid Evaluation of the Debromination Mechanism of Eosin in Oil Paint by Direct Analysis in Real Time and Direct Infusion-Electrospray Ionization Mass Spectrometry*. Anal Chem, 2019. **91**(16): p. 10856-10863.
47. Alvarez-Martin, A., G.A. Newsome, and K. Janssens, *High-Resolution Mass Spectrometry and Nontraditional Mass Defect Analysis of Brominated Historical Pigments*. Anal Chem, 2021. **93**(44): p. 14851-14858.
48. Lech, K., et al., *Early synthetic dyes--a challenge for tandem mass spectrometry*. J Mass Spectrom, 2013. **48**(2): p. 141-7.
49. Vanmeert, F., et al., *Transmission and Reflection Mode Macroscopic X-ray Powder Diffraction Imaging for the Noninvasive Visualization of Paint Degradation in Still Life Paintings by Jan Davidsz. de Heem*. Anal Chem, 2019. **91**(11): p. 7153-7161.
50. *Volume Weight and Pigment to Oil Ratios*. Just paint.
51. International, A., <2002.Standard Test Method for oil absorption of pigments by spatula rub.PDF>. 2002.
52. Chieli, A., et al., *New insights into the fading mechanism of Geranium lake in painting matrix*". Dyes and Pigments, 2020. **181**.
53. Pirok, B.W.J., et al., *Characterization of Dye Extracts from Historical Cultural-Heritage Objects Using State-of-the-Art Comprehensive Two-Dimensional Liquid Chromatography and Mass Spectrometry with Active Modulation and Optimized Shifting Gradients*. Anal Chem, 2019. **91**(4): p. 3062-3069.

## 15. Appendix

Table 19. Materials used in the eosin syntheses

Materials used	
Eosin Y	<a href="https://www.sigmaaldrich.com/BE/en/substance/eosiny6478915086949">https://www.sigmaaldrich.com/BE/en/substance/eosiny6478915086949</a>
Sodium hydroxide	<a href="https://www.sigmaaldrich.com/BE/en/product/sigald/s5881">https://www.sigmaaldrich.com/BE/en/product/sigald/s5881</a>
Aluminum chloride hexahydrate	<a href="https://www.sigmaaldrich.com/BE/en/search/237078-100g?focus=products&amp;page=1&amp;perpage=30&amp;sort=relevance&amp;term=237078-100g&amp;type=product">https://www.sigmaaldrich.com/BE/en/search/237078-100g?focus=products&amp;page=1&amp;perpage=30&amp;sort=relevance&amp;term=237078-100g&amp;type=product</a>
Madder roots	<a href="https://www.kremer-pigmente.com/en/shop/dyes-vegetable-color-paints/37201-madder-roots-ground-with-pieces.html">https://www.kremer-pigmente.com/en/shop/dyes-vegetable-color-paints/37201-madder-roots-ground-with-pieces.html</a>
Aluminum potassium sulfate dodecahydrate	<a href="https://www.sigmaaldrich.com/IT/it/product/sial/a7210?gclid=Cj0KCQjwof6WBhD4ARIsAOi65ahBR66XGOyysG4bBGMRBZMRtgUlejhgBG_4mNEXcyLAYq0IM1-OBgVsaAkSweALw_wcB">https://www.sigmaaldrich.com/IT/it/product/sial/a7210?gclid=Cj0KCQjwof6WBhD4ARIsAOi65ahBR66XGOyysG4bBGMRBZMRtgUlejhgBG_4mNEXcyLAYq0IM1-OBgVsaAkSweALw_wcB</a>
Potash	<a href="https://www.kremer-pigmente.com/en/shop/solvents-chemicals-additives/64040-potash.html">https://www.kremer-pigmente.com/en/shop/solvents-chemicals-additives/64040-potash.html</a>
Brazilwood shavings	<a href="https://www.kremer-pigmente.com/en/shop/dyes-vegetable-color-paints/natural-organic-dyes-vegetable-color-paints/36150-brazilwood-shavings.html">https://www.kremer-pigmente.com/en/shop/dyes-vegetable-color-paints/natural-organic-dyes-vegetable-color-paints/36150-brazilwood-shavings.html</a>
Chalk	<a href="https://www.kremer-pigmente.com/en/shop/fillers-building-materials/58340-alabaster-plaster.html">https://www.kremer-pigmente.com/en/shop/fillers-building-materials/58340-alabaster-plaster.html</a>
Aluminum potassium sulfate dodecahydrate	<a href="https://www.sigmaaldrich.com/IT/it/product/sial/a7210?gclid=Cj0KCQjwof6WBhD4ARIsAOi65ahBR66XGOyysG4bBGMRBZMRtgUlejhgBG_4mNEXcyLAYq0IM1-OBgVsaAkSweALw_wcB">https://www.sigmaaldrich.com/IT/it/product/sial/a7210?gclid=Cj0KCQjwof6WBhD4ARIsAOi65ahBR66XGOyysG4bBGMRBZMRtgUlejhgBG_4mNEXcyLAYq0IM1-OBgVsaAkSweALw_wcB</a>
Cochineal	<a href="https://www.kremer-pigmente.com/en/shop/pigments/42100-carmine-naccarat.html">https://www.kremer-pigmente.com/en/shop/pigments/42100-carmine-naccarat.html</a>

Table 20. Materials used in the hydro cerussite synthesis

Materials used	
Ammonia solution	<a href="https://www.sigmaaldrich.com/BE/en/product/mm/105432?gclid=Cj0KCQiA09eQBhCxARIsAAYRiykMjNW5o2FsDB6skpU2YIMvHBMJThdUakM1fAa2k9H4dhfJmL1VVaYaAvaUEALw_wcB">https://www.sigmaaldrich.com/BE/en/product/mm/105432?gclid=Cj0KCQiA09eQBhCxARIsAAYRiykMjNW5o2FsDB6skpU2YIMvHBMJThdUakM1fAa2k9H4dhfJmL1VVaYaAvaUEALw_wcB</a>
Sodium hydroxide	<a href="https://be.vwr.com/store/product?keyword=27771.290">https://be.vwr.com/store/product?keyword=27771.290</a>
Lead Nitrate	<a href="https://www.fishersci.be/shop/products/lead-ii-nitrate-99-analysis-thermo-scientific/p-7077232#?keyword=10099-74-8">https://www.fishersci.be/shop/products/lead-ii-nitrate-99-analysis-thermo-scientific/p-7077232#?keyword=10099-74-8</a>

Table 21. Used materials for embedding

Used materials	
Tecnovit 5000	<a href="https://www.kulzer-technik.com/en_kt/kt/metallographie/produktbereiche/verbrauchsmaterialien_einbetten_1/technovit_5000.aspx">https://www.kulzer-technik.com/en_kt/kt/metallographie/produktbereiche/verbrauchsmaterialien_einbetten_1/technovit_5000.aspx</a>
Technovit 4004	<a href="https://www.kulzer-technik.com/en_kt/kt/metallographie/produktbereiche/verbrauchsmaterialien_einbetten_1/technovit_4004.aspx">https://www.kulzer-technik.com/en_kt/kt/metallographie/produktbereiche/verbrauchsmaterialien_einbetten_1/technovit_4004.aspx</a>
Acrifix Liquid	<a href="https://e-shop.struers.com/US/EN/products/Mounting/Cold_mounting_resin?sortById=1">https://e-shop.struers.com/US/EN/products/Mounting/Cold_mounting_resin?sortById=1</a>
VersoCit-2 Liquid	<a href="https://e-shop.struers.com/US/EN/products/Mounting/Cold_mounting_resin/VersoCit-2_Liquid_1_I(40200091).aspx">https://e-shop.struers.com/US/EN/products/Mounting/Cold_mounting_resin/VersoCit-2_Liquid_1_I(40200091).aspx</a>
Technovit 2000 LC	<a href="https://www.kulzer-technik.com/en_kt/kt/metallographie/produktbereiche/verbrauchsmaterialien_einbetten_1/technovit_2000lc.aspx">https://www.kulzer-technik.com/en_kt/kt/metallographie/produktbereiche/verbrauchsmaterialien_einbetten_1/technovit_2000lc.aspx</a>

Table 22. Attribution peaks for ATR-FTIR analyses for synthesized eosin products.

Eosin Y		Eosin (average between the three samples)	
Signal [ $cm^{-1}$ ]	Attribution	Signal [ $cm^{-1}$ ]	Attribution
3467,9 (s)	OH-Br		
3192,3 (br)	$\nu(CH_{aromatic})$	3177,0 (br)	$\nu(CH_{aromatic})$
1750,9 (s)(i)	$\nu(C=O_{lactone})$	3060,3 (sh)	$\nu(CH)$
1464,1 (i)	$\delta(CH)$	1557,0	$\nu(C=O)$
1420,0 (i)	$\nu(C=O)$	1435,0 (i)	$\nu(C=O_{carboxylate})$
1209,7 (i)	$\nu(C(C=O)O)$	1335,0 (i)	$\nu(C=O_{ketone})$
1157,4	$\nu(CH_{xanthene})$	1239,9	$\nu(C-O_{xanthene})$
1114,7 (i)	$\nu(CH_{xanthene})$	1177,0	
906,0		1063,0	
872,5	$\nu(CH_{xanthene})$	978,0 (s) (i)	
745,3		761,5	$\nu(CH_{xanthene})$
695,1	$\nu(C-Br)$	570,0	$\nu(CH_{xanthene})$
613,16	$\nu(C-Br)$		
571,44	$\nu(CH_{xanthene})$		

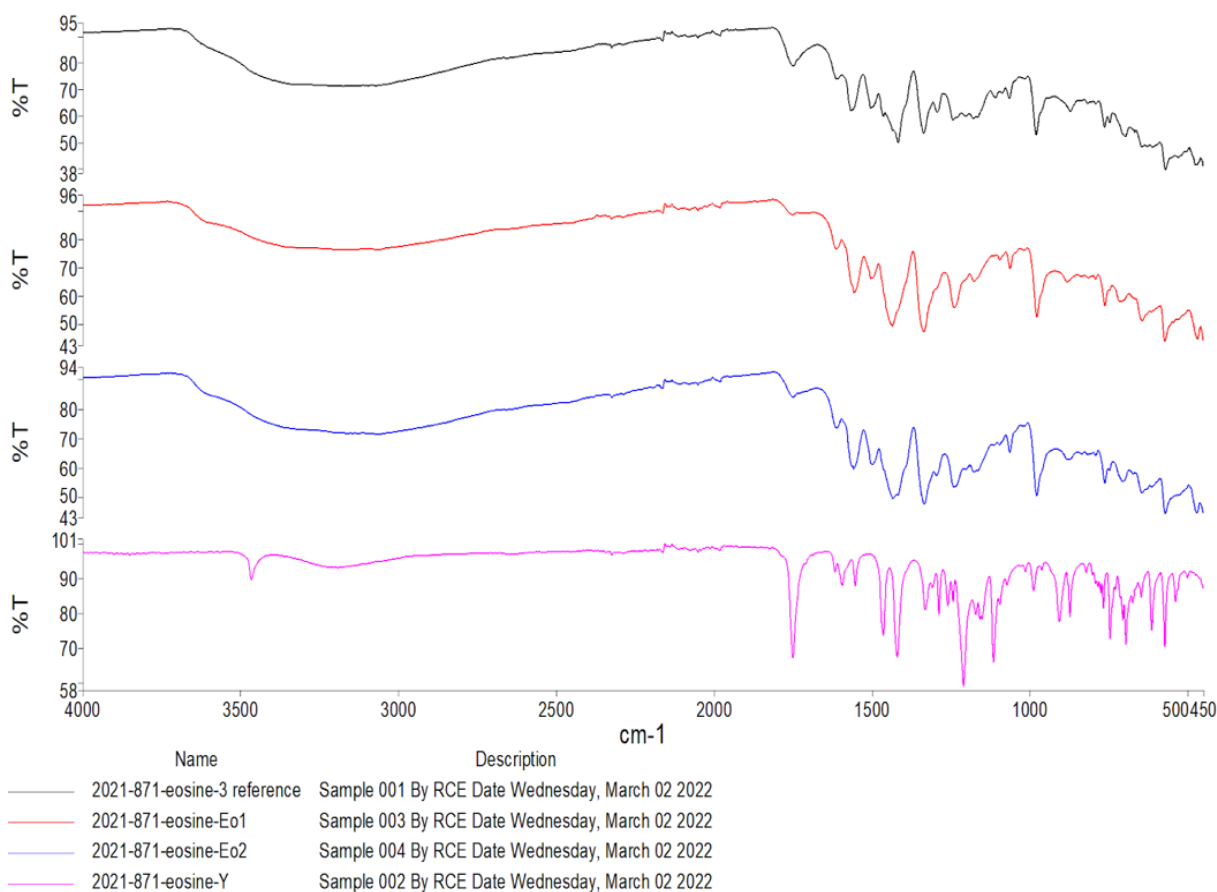
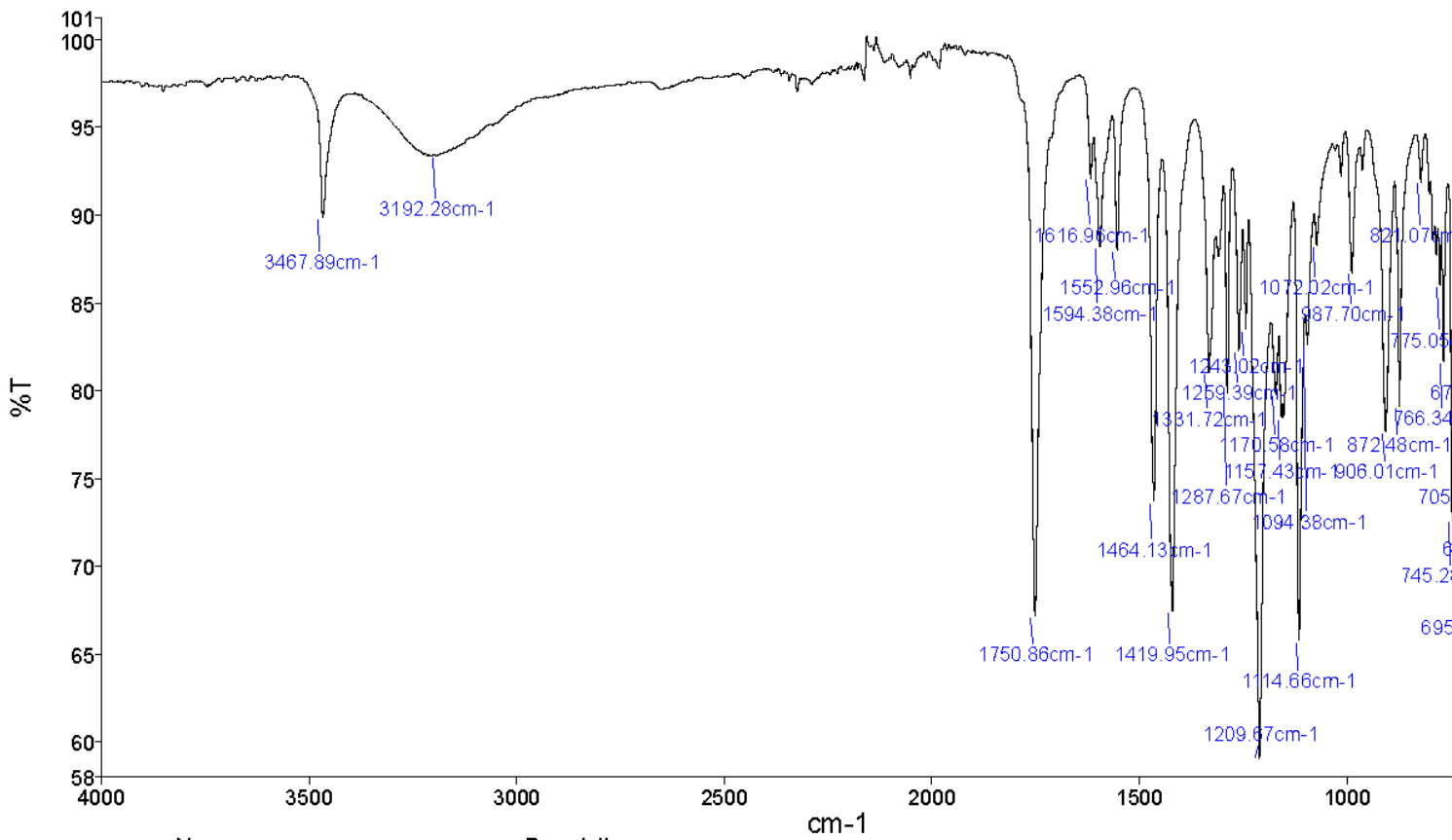
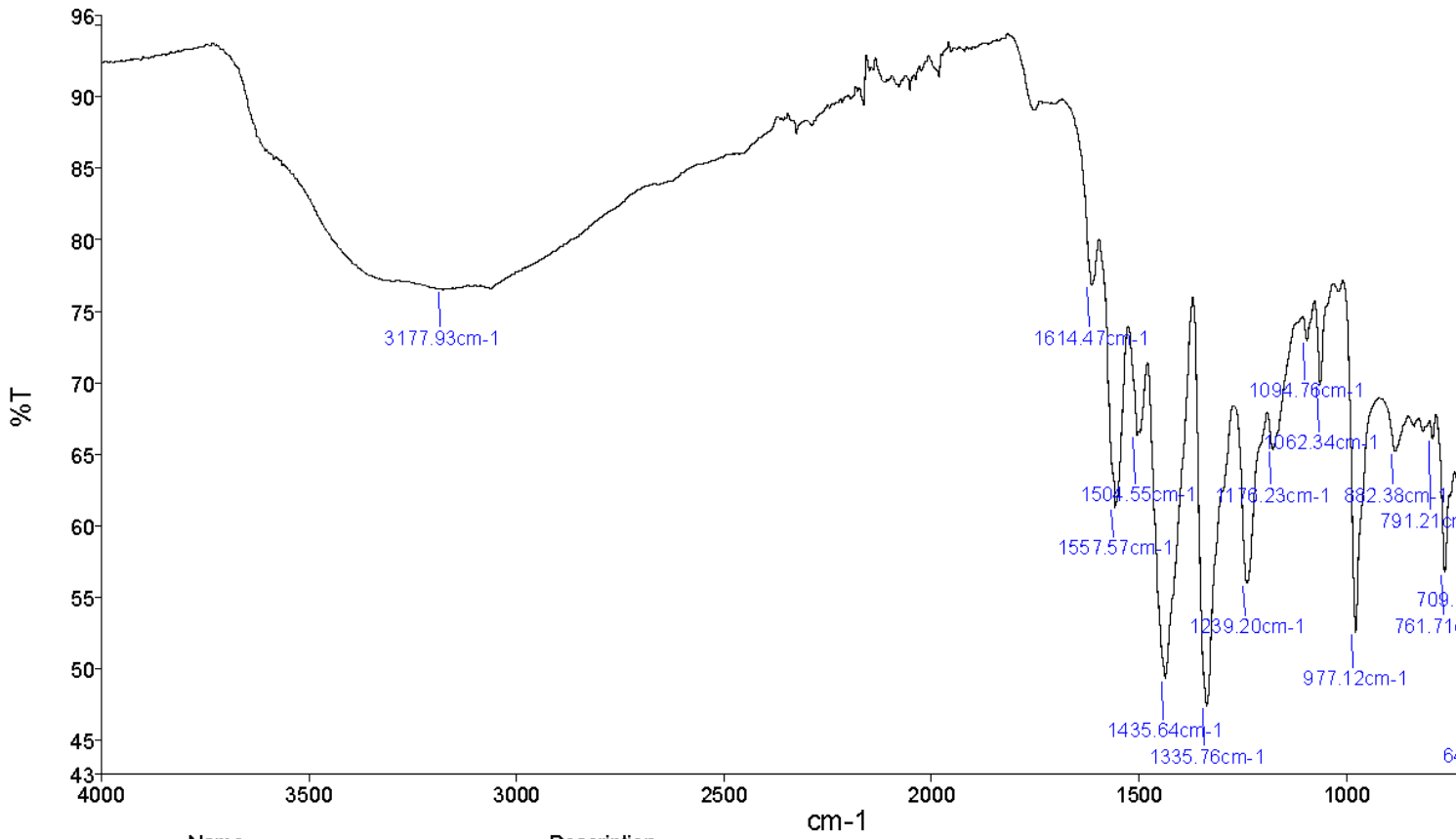


Figure 68. ATR-FTIR comparison between all the spectra (purple) eosin Y and eosin firstly (red), secondly (blue) and thirdly (black) synthesized



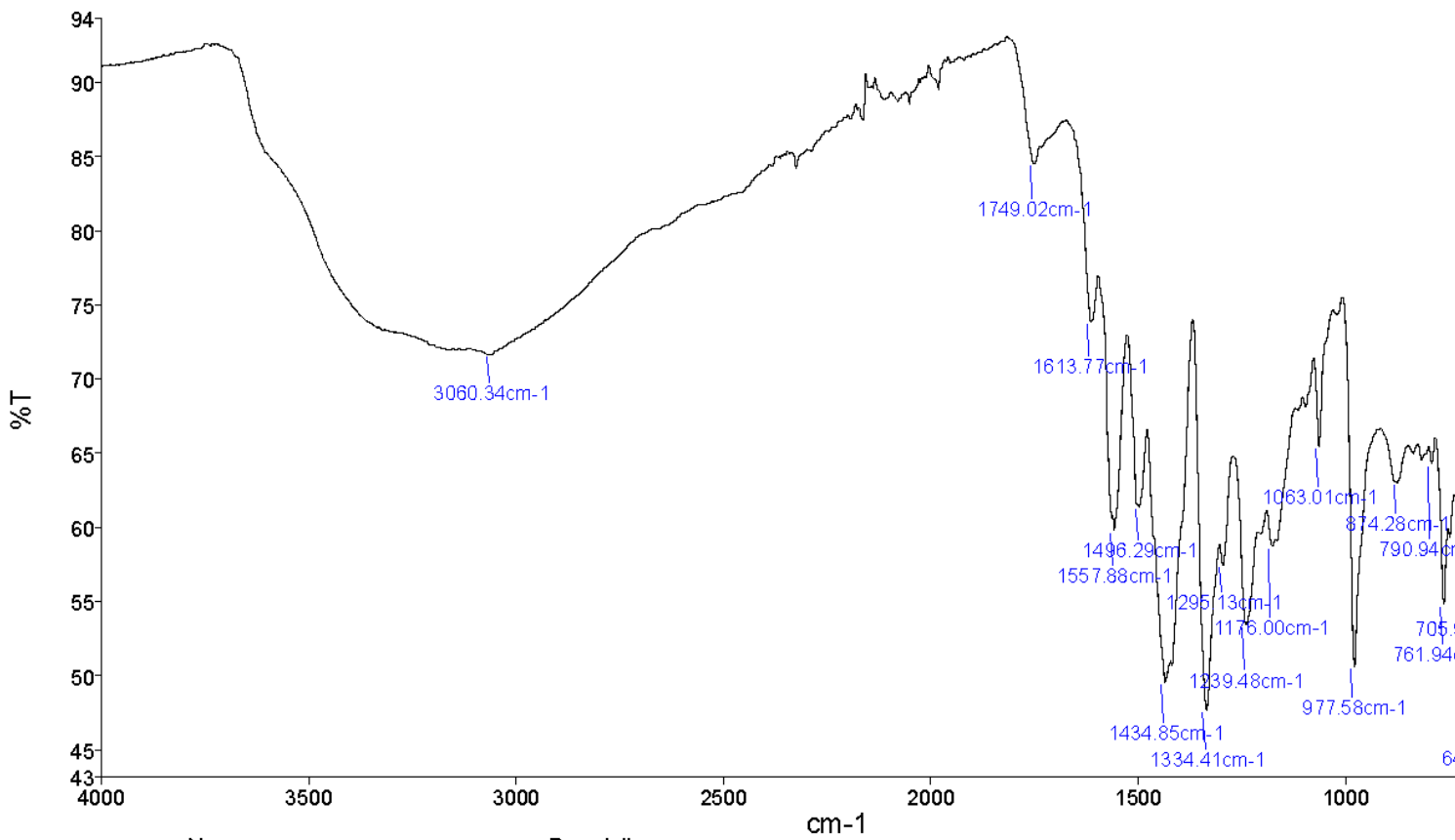
Name: 2021-871-eosine-Y Description: Sample 002 By RCE Date Wednesday, March 02 2022

Figure 69. ATR-FTIR spectrum of eosin Y



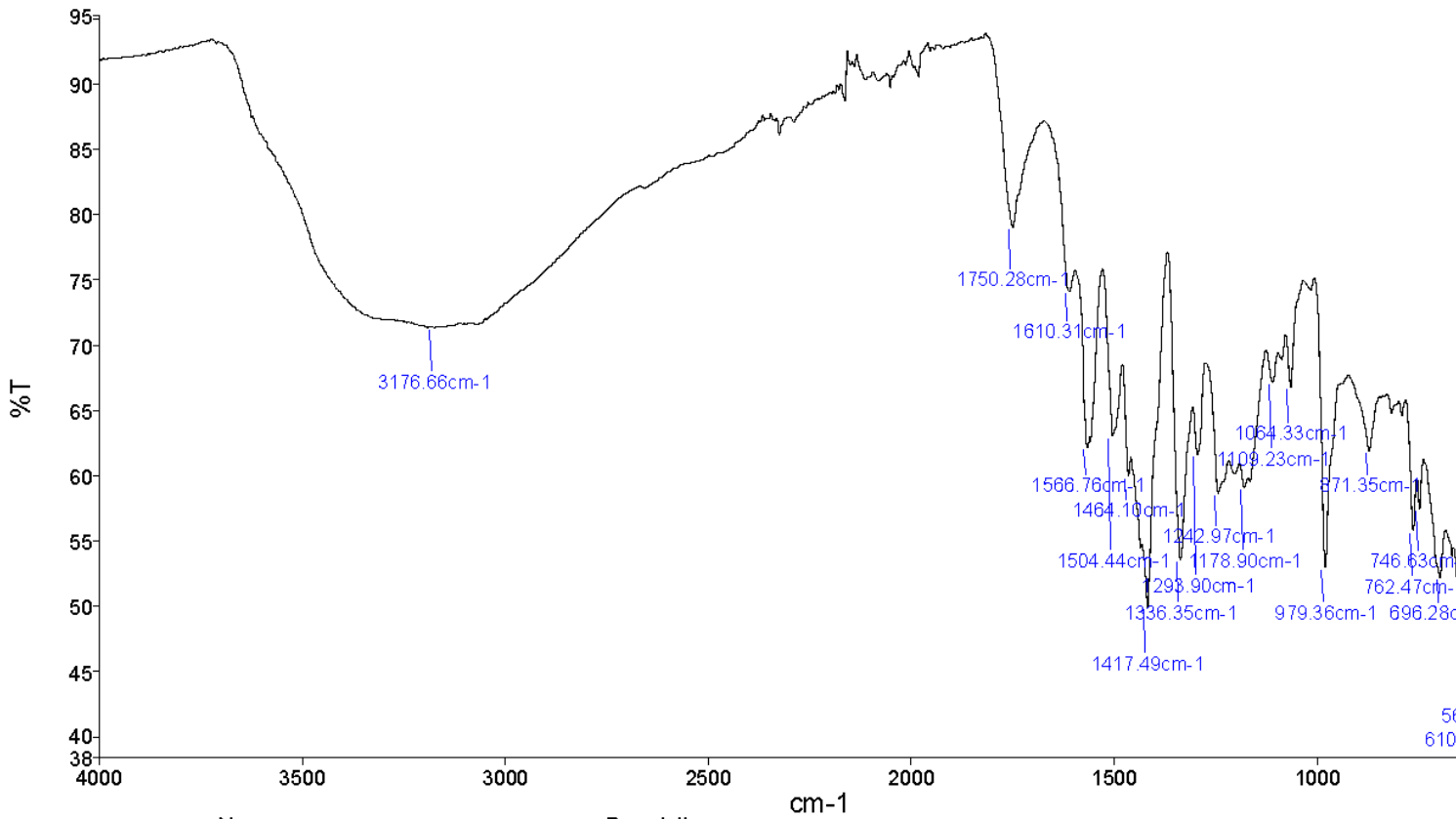
Name: 2021-871-eosine-Eo1 Description: Sample 003 By RCE Date Wednesday, March 02 2022

Figure 70- ATR-FTIR spectrum first synthesized eosin



Name: 2021-871-eosine-Eo2    Description: Sample 004 By RCE Date Wednesday, March 02 2022

Figure 71. ATR-FTIR spectrum of secondly synthesized eosin



Name: 2021-871-eosine-3 reference    Description: Sample 001 By RCE Date Wednesday, March 02 2022

Figure 72. ATR-FTIR spectrum of thirdly synthesized eosin

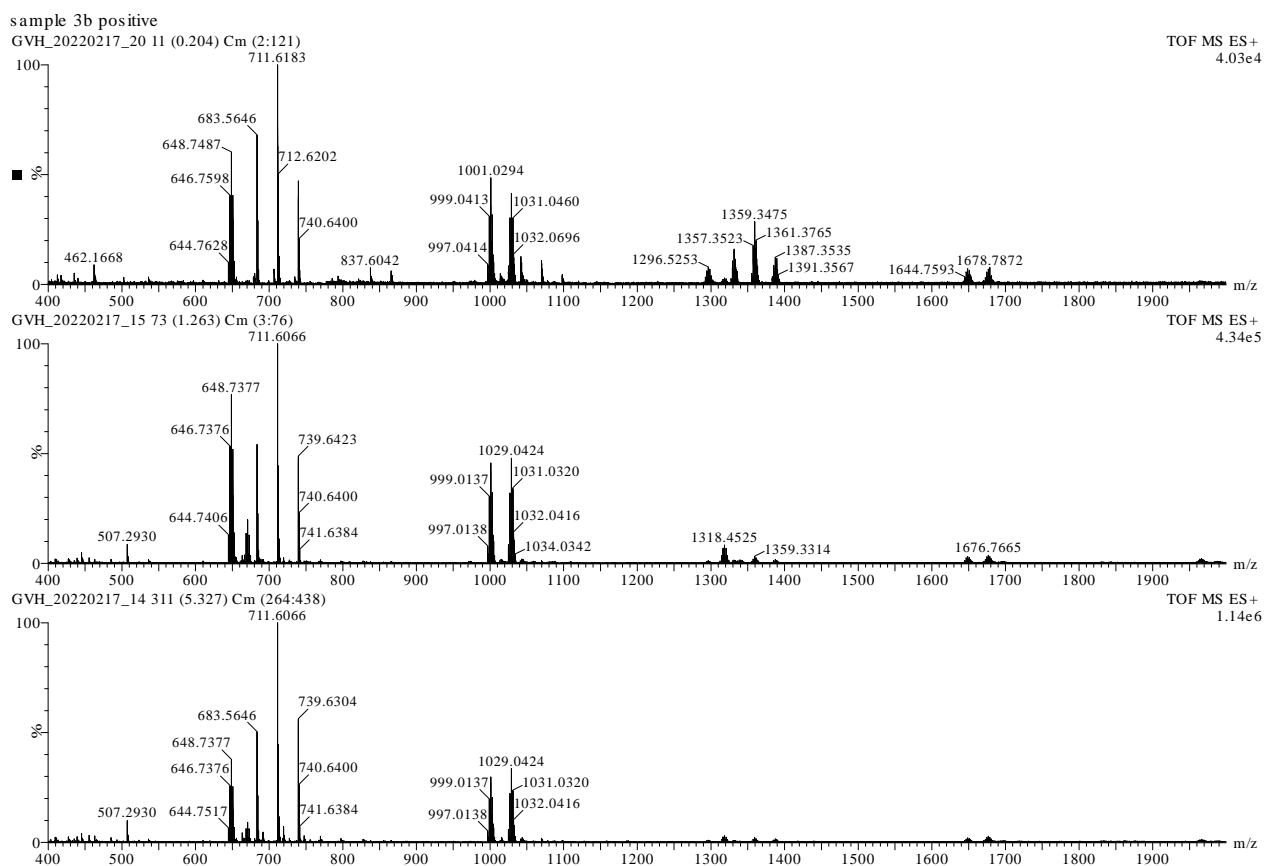


Figure 73. TOF-MS-ES+ mass spectrum of synthesized eosin products

Table 23. Attribution of the main species of the spectra of the secondly synthesized eosin







Assigned code	Assigned formula	Observed m/z	Theoretical monoisotopic m/z
	$[\text{C}_{18}\text{H}_7\text{O}_3\text{Br}_3]^+$	507,29	507,77685
$\text{EoBr}_4^+$	$[\text{C}_{20}\text{H}_9\text{O}_5\text{Br}_4]^+$	648,74	648,71428
$\text{EoBr}_4\text{Na}^+$	$[\text{C}_{20}\text{H}_8\text{O}_5\text{Br}_4\text{Na}]^+$	670,71	670,69622
		711,61	
		739,64	
$(\text{Eo})(\text{EoBr}_4)\text{Na}^+$	$[\text{C}_{40}\text{H}_{20}\text{O}_{10}\text{Br}_4\text{Na}]^+$	1001,02	1002,76472
$(\text{Eo})(\text{EoBr}_4)\text{Al}^+$	$[\text{C}_{40}\text{H}_{15}\text{O}_{10}\text{Br}_4\text{Al}]^+$		1002,72519
$(\text{Eo-Me})(\text{EoBr}_4)(\text{OH})\text{Na}^+$	$[\text{C}_{41}\text{H}_{19}\text{O}_{11}\text{Br}_4\text{Na}]^+$	1029,04	1029,75182
$(\text{Eo-Me})(\text{EoBr}_4)(\text{OH})\text{Al}^+$	$[\text{C}_{41}\text{H}_{15}\text{O}_{11}\text{Br}_4\text{Al}]^+$		1029,71229
$(\text{EoBr}_4)_2\text{Na}^+$	$[\text{C}_{40}\text{H}_{16}\text{O}_{10}\text{Br}_8\text{Na}]^+$	1318,45	1318,40267
$(\text{EoBr}_4)_2\text{Al}^+$	$[\text{C}_{40}\text{H}_{12}\text{O}_{10}\text{Br}_8\text{Al}]^+$		1318,36314
$(\text{EoBr}_4)_2(\text{H}_2\text{O})\text{Na}_2^+$	$[\text{C}_{40}\text{H}_{18}\text{O}_{11}\text{Br}_8\text{Na}_2]^+$	1359,33	1359,40301
$(\text{Eo})(\text{EoBr}_4)_2\text{Na}^+$	$[\text{C}_{60}\text{H}_{22}\text{O}_{15}\text{Br}_8\text{Na}]^+$	1644,76	1644,42422
$(\text{Eo})(\text{EoBr}_4)_2\text{Al}^+$	$[\text{C}_{60}\text{H}_{18}\text{O}_{15}\text{Br}_8\text{Al}]^+$		1644,38469
$(\text{Eo-Me})(\text{OH})(\text{EoBr}_4)_2\text{Na}^+$	$[\text{C}_{61}\text{H}_{26}\text{O}_{16}\text{Br}_8\text{Na}]^+$	1676,77	1676,45044
$(\text{Eo-Me})(\text{OH})(\text{EoBr}_4)_2\text{Al}^+$	$[\text{C}_{61}\text{H}_{22}\text{O}_{16}\text{Br}_8\text{Al}]^+$		1676,41091















Table 24. Pictures table of all the dried samples eosin-based

Cobalt blue : Eosin						
100 : 0	>99 : <1	99 : 1	95 : 5	50 : 50	5 : 95	0 : 100
						
Vermilion : Eosin						
100 : 0	>99 : <1	99 : 1	95 : 5	50 : 50	5 : 95	0 : 100
						
Lead white : Eosin						
100 : 0	>99 : <1	99 : 1	95 : 5	50 : 50	5 : 95	0 : 100
						
Zinc white : Eosin						
100 : 0	>99 : <1	99 : 1	95 : 5	50 : 50	5 : 95	0 : 100
						

Table 25. Pictures table of dried samples cochineal-based

Cobalt blue : Cochineal						
100 : 0	>99 : <1	99 : 1	95 : 5	50 : 50	5 : 95	0 : 100
						
Vermilion : Cochineal						
100 : 0	>99 : <1	99 : 1	95 : 5	50 : 50	5 : 95	0 : 100

						
Lead white : Cochineal						
100 : 0	>99 : <1	99 : 1	95 : 5	50 : 50	5 : 95	0 : 100
						
Zinc white : Cochineal						
100 : 0	>99 : <1	99 : 1	95 : 5	50 : 50	5 : 95	0 : 100
